

GANs with First-Order Greedy Discriminators

Vijay Keswani
Yale University

Oren Mangoubi
WPI

Sushant Sachdeva
University of Toronto

Nisheeth K. Vishnoi
Yale University

Abstract

We propose a variant of the standard min-max framework for GANs to learn a distribution, where the discriminator can update its strategy in a greedy manner until it reaches a first-order stationary point. We give an algorithm to train such a GAN and show that it provably converges from any initial point to an approximate local equilibrium for this framework. Our algorithm runs in time polynomial in the smoothness parameters of the loss function and independent of the dimension, and allows for loss functions that can be nonconvex and nonconcave in the parameters of the generator and discriminator. Empirically, GANs trained using our algorithm consistently learn a greater number of modes than gradient descent-ascent (GDA), optimistic mirror descent (OMD), and unrolled GANs when applied to a synthetic Gaussian mixture dataset. Moreover, they perform significantly better on CIFAR-10 than OMD and GDA when comparing the mean and standard deviation of the Inception Score respectively.

Contents

1	Introduction	3
2	Theoretical results	6
2.1	Framework and equilibrium	6
2.2	Algorithm	7
2.3	Convergence guarantees	10
3	Key ideas in the proof	11
4	Empirical results	11
5	Proof of Theorem 2.4	15
5.1	Step 1: Bounding the number of gradient, function, and sampling oracle evaluations.	16
5.2	Step 2: Proving the output (x^*, y^*) of Algorithm 1 is an approximate local equilibrium for our framework.	19
6	Conclusion and future directions	22
A	Extension to functions with compact convex support	27
A.1	Projected gradient algorithm for compactly supported loss	27
A.2	Simple application to bi-linear losses	27
A.3	Comparison of local equilibrium and global min-max in the compactly supported convex-concave setting.	29
B	Additional empirical details and results for Gaussian mixture and CIFAR-10 datasets	31
B.1	Simulation setup for Gaussian mixture and CIFAR-10 datasets	31
B.2	Additional simulation results for Gaussian mixture and CIFAR-10 datasets	35
C	Empirical results for MNIST dataset	36
D	Randomized acceptance rule with decreasing temperature	38

1 Introduction

Learning to generate new data with similar statistics to a given dataset is a central problem in machine learning due to its numerous applications to data augmentation [12], unsupervised learning problems such as clustering [30] and learning 3-dimensional object representations from 2-dimensional images [34], and semi-supervised learning [20]. In recent years, many solutions to this problem have employed generative adversarial networks or GANs.

GANs, loosely defined, consist of a generator network \mathcal{G}_x and discriminator network \mathcal{D}_y with trainable parameters (x, y) in some (convex) domain $\mathcal{X} \times \mathcal{Y} \subseteq \mathbb{R}^d \times \mathbb{R}^d$. The generator takes as input Gaussian noise and outputs “fake” generated images (or datapoints). The discriminator seeks to challenge the generator by distinguishing between the generated images and dataset images. The discriminator’s error is measured by a loss function $f(x, y)$. The goal of a GAN framework is for the generator to learn the dataset’s distribution, by training the generator to generate images which are difficult for the discriminator to tell apart from the images in the dataset. In particular, the widely used min-max GAN framework [14] models the problem of finding the best generator and discriminator as a solution to the following optimization problem:

$$\min_{x \in \mathcal{X}} \max_{y \in \mathcal{Y}} f(x, y). \quad (1)$$

Unfortunately, there is a lack of algorithms with convergence guarantees for this min-max framework if one allows for loss functions which are nonconvex/nonconcave in the generator/discriminator parameters. This lack of convergence guarantees can be a serious problem in practice, since popular algorithms such as gradient descent-ascent oftentimes fail to converge, and GANs trained with these algorithms and can suffer from issues such as cycling [2] and “mode collapse” [11, 8, 38].

Since min-max optimization includes minimization (and maximization) as special cases, it is intractable for general nonconvex/nonconcave functions. Motivated by the success of a long line of results which show efficient convergence of minimization algorithms to various (approximate) local minimum notions, e.g., [33, 13, 1], previous works have sought to extend these ideas of local minimum to various (approximate) notions of local min-max point—that is, a point (x^*, y^*) where x^* is a local minimum of $f(\cdot, y^*)$ and y^* is a local maximum of $f(x^*, \cdot)$ —in the hope that this will allow for algorithms with convergence guarantees to such points. Unfortunately, these works make strong assumptions on f , for instance assuming $f(x, y)$ is concave in y , or that their algorithm is provided with a starting point such that its underlying dynamical system converges (see Related work). It remains a challenge to develop algorithms for training GANs which converge efficiently to an equilibrium for even a local variant of the min-max framework under less restrictive assumptions which are standard when analyzing convergence of optimization algorithms to local minima.

Our contributions. We propose a variant of the min-max framework for GANs to learn a distribution, which allows the discriminator to update y in a “greedy” manner (Section 2.1). This greedy restriction models discriminators that make updates via a class of first-order algorithms popular in deep learning, such as gradient ascent, which can make updates far from the current value of y when run for multiple steps. Roughly speaking, from the current point (x, y) , our framework allows the discriminator to update y along *any* continuous path, along which the loss $f(x, \cdot)$ is nondecreasing. In the special case when f is convex-concave and \mathcal{X}, \mathcal{Y} are compact, we show that our framework is equivalent to the (global) min-max framework (see Appendix A).

Our main contribution is a new algorithm for training GANs in this framework (Algorithm 1). We prove that it converges from any initial point to an approximate local equilibrium for this framework (Definition 2.2) on any smooth and bounded loss f , in a number of gradient evaluations polynomial in d and the smoothness parameters of f (Theorem 2.4). We show how this result leads to a practical algorithm for training GANs with cross entropy loss, whose per-step complexity and memory requirement is similar to GDA.

Empirically, GANs trained using our practical algorithm consistently learn a greater number of modes than gradient descent-ascent (GDA), optimistic mirror descent (OMD), and unrolled GANs when applied to a synthetic Gaussian mixture dataset (Table 1 in Section 4). On CIFAR-10, in comparison to OMD, they achieve Inception Scores with a significantly higher mean (Table 2) and, visually, the images produced by our algorithm on CIFAR-10 are of significantly higher quality than those of OMD (Figure 2). Moreover, in comparison to GDA, the inception scores for our algorithm on CIFAR-10 have significantly lower standard deviation than for GDA. This lower standard deviation is reflected by the fact that, visually, our algorithm produces high-quality images more consistently than GDA, which produces poor-quality images in some of the runs.

Related work. *GAN frameworks.* In addition to the min-max and local min-max frameworks, prior works have proposed other frameworks for GANs. For instance, in the Nash GAN framework (e.g., [36]), the goal is to find $(x^*, y^*) \in \mathcal{X} \times \mathcal{Y}$ such that $x^* \in \arg \min_{x \in \mathcal{X}} f(x, y^*)$ and $y^* \in \arg \max_{y \in \mathcal{Y}} f(x^*, y)$. This is in contrast to our framework (and to the min-max framework), where the generator seeks to decrease an objective function which anticipates the response of the discriminator. Moreover, as with the min-max framework, the Nash GAN framework includes minimization (and maximization) as a special case and is intractable for general nonconvex/nonconcave f .

In the Wasserstein GAN (WGAN) framework, one seeks to find a generator with parameters x that minimizes the Wasserstein distance between the distribution of the generated images and the dataset [3]. A second neural network (roughly analogous to the discriminator) with parameters y is used to compute the Wasserstein distance, and in practice this is done by making use of the dual formulation of the WGAN. Roughly, in its dual form, the WGAN framework corresponds to a special case of the min-max GAN framework if one sets \mathcal{Y} to be such that \mathcal{D}_y is 1-Lipschitz for all $y \in \mathcal{Y}$ and the loss f to be the WGAN loss $f(x, y) = \mathcal{D}_y(\zeta) - \mathcal{D}_y(\mathcal{G}_x(\xi))$, where ζ is sampled from the data, and $\xi \sim N(0, I_d)$. Thus, since our framework is a variant of min-max GANs, in the special case where one implements our framework with the above choices of loss function, domain \mathcal{Y} , and discriminator \mathcal{D}_y , our framework can also be viewed as a variant of the WGAN framework.

In addition to the local min-max framework, a related notion of local minimax point was proposed in [17], where the discriminator is able to choose its move after the generator reveals its move. In both the local min-max and local minimax frameworks the discriminator is restricted to move in a small ball around the current point y . In contrast, in our framework, the discriminator can move much farther, as long as it is following a path along which the loss function increases.

Our GAN framework is inspired by the work of [24], who introduce a robust optimization model which can be viewed as an alternative to min-max optimization, and is based on a “second-order” version of the greedy paths we use here. Their paths model a class of second-order optimization algorithms which require access to their objective functions’ Hessian. However, it is generally not feasible to compute the Hessian in GAN applications since d may be very large. For this reason we design our framework for GANs using first-order greedy paths. And, in contrast to the bounds for the algorithm in [24] which depend polynomially on d , the bound on the number of gradient evaluations for our training algorithm is independent of d .

Training GANs. Starting with [14], who use GDA to train min-max GANs, there has been considerable work to develop algorithms for training GANs. One line of work regularizes the discriminator, for instance by applying gradient penalties [15] or spectral normalization of the discriminator’s neural network [28]. Another line of work focuses on designing training algorithms that mitigate non-convergence behavior such as cycling when training GANs. [9] propose the application of OMD for training GANs, an algorithm first introduced in [35] in the context of convex-concave min-max optimization, and show that OMD can mitigate cycling when training GANs with Wasserstein loss. In contrast to both GDA and OMD, which at each iteration allow the generator and discriminator to make a small update roughly proportional to their respective gradients, our algorithm empowers the discriminator to make large updates at each iteration. [27] introduced Unrolled GANs, where the generator optimizes an “unrolled” loss function that allows the generator to simulate a fixed number of discriminator updates. While this has some similarity to our algorithm there are two important distinctions: 1) the discriminator in Unrolled GANs may not reach a first-order stationary point, and hence their algorithm does not come with any convergence guarantees, and 2) unlike our algorithm, the implementation of the generator in Unrolled GANs requires memory that grows with the number of discriminator steps, limiting its scalability. We observe that our algorithm, applied to training GANs, trains stably and avoids mode collapse, while achieving a training time per iteration and memory requirements that are similar to GDA and OMD, and much lower than Unrolled GANs [27] (see also Section 6).

Convergence guarantees. Several works have studied the convergence properties of GDA dynamics [31, 26, 10], and established that GDA suffers from severe limitations: GDA can exhibit rotation around some points, or otherwise fail to converge. To address these convergence issues for GDA, multiple works have analyzed algorithms based on Optimistic Mirror Descent (OMD), Extra-gradient methods, or similar approaches. For instance, [9] guarantee convergence for OMD to a global min-max point on a bilinear loss $f(x, y) = x^\top A y$ in a number of iterations that is polynomial in the condition number of A . And [29] also show convergence of extra-gradient methods on strongly convex-strongly concave losses. However, losses arising in most GANs are nonconvex-nonconcave. [25] show asymptotic convergence of OMD under a “coherence” assumption which requires that $(-\nabla_x f(x, y), \nabla_y f(x, y))$ never points away from any of the global min-max points of f . However, there are many simple functions such as $f(x, y) = \sin(x)$ which do not satisfy this coherence assumption.

For this reason, multiple works show convergence to (approximate versions of) a local min-max point. For instance [16] prove convergence of finite-step GDA to a local min-max point, under the assumption that their algorithm is provided with an initial point such that the underlying continuous dynamics converge to a local min-max point. And other works (e.g., [32, 23]) provide convergence guarantees to an approximate local min-max point when f may be nonconvex in x , but concave in y . However, since y are the parameters of the discriminator neural network, loss functions arising in GANs need not even be concave in y . In contrast to the above works, our algorithm is guaranteed to converge for any nonconvex-nonconcave loss, from any starting point, in a number of gradient evaluations polynomial in d , L and b if f is b -bounded with L -Lipschitz gradient. Such smoothness/Lipschitz bounds are standard in convergence guarantees for optimization algorithms [7, 33, 13, 40].

Finally, while we state our algorithm for unconstrained loss functions, we show how to extend it to loss functions with compact convex domain (Appendix A). In particular, when applied to compactly supported bilinear loss functions, our algorithm can be shown to converge to a point near the global min-max point (Appendix A.2).

2 Theoretical results

2.1 Framework and equilibrium

We present a variant of the min-max framework, which empowers the discriminator to update y in a “greedy” manner. More specifically, we restrict the discriminator to update the current point (x, y) to any point in a set $P(x, y)$ consisting of the endpoints of paths in \mathcal{Y} initialized at y along which $f(x, \cdot)$ is nondecreasing. These paths model the paths taken by a class first-order algorithms, which includes popular algorithms such as gradient ascent. Our framework therefore allows the generator to learn from discriminators which are computationally tractable and yet (in contrast to the local min-max framework) are still empowered to make updates to the value of y which may lead to large increases in $f(x, y)$.

Given a bounded loss $f : \mathcal{X} \times \mathcal{Y} \rightarrow \mathbb{R}$, where $\mathcal{X}, \mathcal{Y} \subseteq \mathbb{R}^d$ are convex, an equilibrium for our framework is a point $(x^*, y^*) \in \mathcal{X} \times \mathcal{Y}$ such that

$$x^* \in \operatorname{argmin}_{x \in \mathcal{X}} (\max_{y \in P(x, y^*)} f(x, y)), \quad (2)$$

$$y^* \in \operatorname{argmax}_{y \in P(x^*, y^*)} f(x^*, y). \quad (3)$$

This is in contrast to the (global) min-max framework of (1) where the maximum is taken over all $y \in \mathcal{Y}$. However, solutions to (2) and (3) may not exist, and even when they do exist, finding such a solution is intractable in general since (2) generalizes nonconvex minimization.

Local equilibrium. We replace the global minimum in (2) with a local minimum, which leads to the following local version of our framework’s equilibrium. A point $(x^*, y^*) \in \mathcal{X} \times \mathcal{Y}$ is a local equilibrium if, for some $\nu > 0$,

$$x^* \in \operatorname{argmin}_{x \in B(x^*, \nu) \cap \mathcal{X}} \left(\max_{y \in P(x, y^*)} f(x, y) \right) \quad (4)$$

$$y^* \in \operatorname{argmax}_{y \in P(x^*, y^*)} f(x^*, y), \quad (5)$$

where $B(x^*, \nu)$ denotes the ball of radius ν centered at x^* .

Approximate local equilibrium. Previous works for local minimization on smooth non-convex objectives oftentimes prove convergence to approximate first- (or second)-order stationary points—points where, roughly speaking, the magnitude of the gradient (and the eigenvalues of the Hessian) are bounded by some positive number (see e.g. [33]). We would like to approximately solve (4) and (5) in a similar manner. Towards this end, for a given $\varepsilon > 0$, we replace the set of endpoints of non-decreasing continuous paths $P(x, y^*)$ in Equations (4) and (5) with the set $P_\varepsilon(x, y^*)$ of endpoints of paths starting at y^* along which $f(x, \cdot)$ increases at some “rate” at least $\varepsilon > 0$; in particular this means that any y^* satisfying (5) would be an approximate first-order stationary point such that $\|\nabla_y f(x^*, y^*)\| \leq \varepsilon$. Roughly, this corresponds to restricting the discriminator to updating y via any “greedy” algorithm, such as gradient ascent, which increases the value of f at a rate of at least ε . The paths need to be unit-speed for the rate of increase to be well-defined.

Definition 2.1. For any $x \in \mathcal{X}$, $y \in \mathcal{Y}$, and $\varepsilon \geq 0$, define $P_\varepsilon(x, y) \subseteq \mathcal{Y}$ to be points $w \in \mathcal{Y}$ s.t. there is a continuous and (except at finitely many points) differentiable path $\gamma(t)$ starting at y , ending at w , and unit-speed, i.e., $\|\frac{d}{dt} \gamma(t)\| \leq 1$, such that at any point on γ ,

$$\frac{d}{dt} f(x, \gamma(t)) \geq \varepsilon. \quad (6)$$

Note that the path γ need not be in the direction of the gradient, and there can potentially be infinitely many such paths starting at y . Moreover, $P_\varepsilon(x, y)$ depends both on x and y since there may be multiple ε -stationary points of $f(x, \cdot)$ and, hence, the set of such points reachable by ε -increasing path depends on x and y .

While we would also like to replace the local minimum in (4) with an approximate stationary point, the *generator's objective*, $\mathcal{L}_\varepsilon(x, y) := \max_{z \in P_\varepsilon(x, y)} f(x, z)$, may not be continuous¹ in x , and thus, gradient-based notions of approximate local minimum do not apply. To bypass this difficulty and to define a notion of approximate local minimum which applies to discontinuous functions, we sample updates to x , and test whether $\mathcal{L}_\varepsilon(\cdot, y)$ has decreased. Formally, given a choice of sampling distribution Q_x (which may depend on x), and $\delta, \omega > 0$, x^* is said to be an approximate local minimum of a (possibly discontinuous) function $g : \mathcal{X} \rightarrow \mathbb{R}$ if $\Pr_{\Delta \sim Q_{x^*}} [g(x^* + \Delta) < g(x^*) - \delta] < \omega$.

Thus, replacing the set P with P_ε in equations 4, 5, and the “exact” local minimum in (4) with an approximate local minimum, we arrive at our equilibrium definition:

Definition 2.2. *Given $\varepsilon, \delta, \omega > 0$ and a distribution $Q_{x,y}$, we say that a point $(x^*, y^*) \in \mathcal{X} \times \mathcal{Y}$ is an approximate local equilibrium for our framework if*

$$\Pr_{\Delta \sim Q_{x^*, y^*}} \left[\max_{y \in P_\varepsilon(x^* + \Delta, y^*)} f(x^* + \Delta, y) < \max_{y \in P_\varepsilon(x^*, y^*)} f(x^*, y) - \delta \right] < \omega, \quad (7)$$

$$y^* \in \operatorname{argmax}_{y \in P_\varepsilon(x^*, y^*)} f(x^*, y). \quad (8)$$

One can set $Q_{x,y}$ to be the standard normal distribution, or, as we do to train GANs, to be the distribution of stochastic gradients with mean $-\nabla_x f(x, y)$ (see Remark 2.3).

2.2 Algorithm

We present a training algorithm for our GAN framework (Algorithm 1), along with the gradient ascent subroutine which it uses to compute discriminator updates (Algorithm 2). In Section 2.3, show that it is able to efficiently find an approximate local equilibrium (Definition 2.2).

We consider bounded loss functions $f : \mathbb{R}^d \times \mathbb{R}^d \rightarrow \mathbb{R}$, where f is an empirical risk loss over m training examples, i.e., $f := \frac{1}{m} \sum_{i \in [m]} f_i$. We assume we are given access to f via a randomized oracle F such that $\mathbb{E}[F] = f$. We call such an oracle a stochastic zeroth-order oracle for f . We are also given randomized oracles G_x, G_y for $\nabla_x f, \nabla_y f$, such that $\mathbb{E}[G_x] = \nabla_x f$, and $\mathbb{E}[G_y] = \nabla_y f$, and call such oracles stochastic gradient oracles for f . These oracles are computed by randomly sampling “batches” $B, B_x, B_y \subseteq [m]$ (iid, with replacement) and returning $F = 1/|B| \sum_{i \in B} f_i$, $G_x = 1/|B_x| \sum_{i \in B_x} \nabla_x f_i$, and $G_y = 1/|B_y| \sum_{i \in B_y} \nabla_y f_i$. For our convergence guarantees, we require the following bounds on standard smoothness parameters for functions $f_i : b$ such that for all i and all x, y , we have $|f_i(x, y)| \leq b$, and such that $\|\nabla f_i(x, y) - \nabla f_i(x', y')\| \leq L\|x - x'\| + L\|y - y'\|$. These bounds imply f is also continuous, b -bounded, and L -gradient-Lipschitz.

¹Consider the example $f(x, y) = \min(x^2 y^2, 1)$. The generator's objective for $\varepsilon > 0$ is $\mathcal{L}_\varepsilon(x, y) = f(x, y)$ if $2x^2 y < \varepsilon$, and 1 otherwise. Thus $\mathcal{L}_{1/2}$ is discontinuous at $(1/2, 1)$.

Algorithm 1 Training algorithm

input: Stochastic zeroth-order oracle F for bounded loss function $f : \mathbb{R}^d \times \mathbb{R}^d \rightarrow \mathbb{R}$ with L -Lipschitz gradient, stochastic gradient oracle G_y with mean $\nabla_y f$
input: A distribution $Q_{x,y}$, and an oracle for sampling from this distribution
input: Initial point (x_0, y_0) , Error parameters $\varepsilon, \omega, \delta > 0$
output: A point (x^*, y^*)
hyperparameters: $\eta > 0$ (learning rate), r_{\max} (maximum number of rejections); τ_1 (for annealing);

- 1: Set $i \leftarrow 0$, $r \leftarrow 0$, $\varepsilon_0 = \frac{\varepsilon}{2}$, $f_{\text{old}} \leftarrow \infty$
- 2: **while** $r \leq r_{\max}$ **do**
- 3: Sample Δ_i from the distribution Q_{x_i, y_i}
- 4: Set $X_{i+1} \leftarrow x_i + \Delta_i$ *{Compute the proposed update for the generator}*
- 5: Run Algorithm 2 with inputs $x \leftarrow X_{i+1}$, $y_0 \leftarrow y_i$, and $\varepsilon' \leftarrow \varepsilon_i \times \frac{1}{1-2\eta L}$ *{Discriminator's update}*
- 6: Set $\mathcal{Y}_{i+1} \leftarrow y_{\text{stationary}}$ to be the output of Algorithm 2.
- 7: Set $f_{\text{new}} \leftarrow F(X_{i+1}, \mathcal{Y}_{i+1})$ *{Compute the new loss value}*
- 8: Set $\text{Accept}_i \leftarrow \text{True}$.
- 9: **if** $f_{\text{new}} > f_{\text{old}} - \frac{\delta}{4}$, **then**
- 10: Set $\text{Accept}_i \leftarrow \text{False}$ with probability $\max(0, 1 - e^{-\frac{i}{\tau_1}})$ *{Decide to accept or reject}*
- 11: **if** $\text{Accept}_i = \text{True}$ **then**
- 12: Set $x_{i+1} \leftarrow X_{i+1}$, $y_{i+1} \leftarrow \mathcal{Y}_{i+1}$ *{accept the proposed x and y updates}*
- 13: Set $f_{\text{old}} \leftarrow f_{\text{new}}$, $r \leftarrow 0$, $\varepsilon_{i+1} \leftarrow \varepsilon_i \times \frac{1}{(1-2\eta L)^2}$
- 14: **else**
- 15: Set $x_{i+1} \leftarrow x_i$, $y_{i+1} \leftarrow y_i$, $r \leftarrow r + 1$, $\varepsilon_{i+1} \leftarrow \varepsilon_i$ *{Reject the proposed updates and track how many successive steps were rejected.}*
- 16: Set $i \leftarrow i + 1$
- 17: **return** $(x^*, y^*) \leftarrow (x_i, y_i)$

Algorithm 2 Stochastic gradient ascent (for discriminator updates)

input: Stochastic gradient oracle G_y for $\nabla_y f$; initial points x, y_0 ; error parameter ε'

output: A point $y_{\text{stationary}}$ which is a first-order ε' -stationary point for $f(x, \cdot)$,

hyperparameters: $\eta > 0$

```
1: Set  $j \leftarrow 0$ , Stop = False
2: while Stop = False do
3:   Set  $g_{y,j} \leftarrow G_y(x, y_j)$ 
4:   if  $\|g_{y,j}\| > \varepsilon'$  then
5:     Set  $y_{j+1} \leftarrow y_j + \eta g_{y,j}$  {Compute update of y-variable}
6:     Set  $j \leftarrow j + 1$ 
7:   else
8:     Set Stop = True
9: return  $y_{\text{stationary}} \leftarrow y_j$ 
```

Overview and intuition of our training algorithm. From the current point (x, y) , our training algorithm first proposes a random update Δ from the given distribution $Q_{x,y}$ to update the generator's parameters to x . In practice, we choose $Q_{x,y}$ to be the distribution of the (scaled) stochastic gradient $-G_x$, although one may implement our algorithm with any choice of distribution $Q_{x,y}$. Then, it updates the discriminator parameters greedily by running gradient ascent using the stochastic gradients G_y until it reaches a first-order ε -stationary point y' , that is, a point where $\|\nabla_y f(x + \Delta, y')\| \leq \varepsilon$. Thus, the point y' satisfies (8). However, our training algorithm still needs to eventually find a pair of points (x^*, y^*) where x^* is an approximate local minimum of the generator's objective $\mathcal{L}_\varepsilon(\cdot, y^*)$ in order to satisfy (7). Moreover, it must also ensure that this new point y^* satisfies (8).

Towards this end, the training algorithm does the following:

- 1) The training algorithm re-uses this same point y' to compute an approximation $f(x + \Delta, y')$ for $\mathcal{L}_\varepsilon(x + \Delta, y)$ in order to have access to the value of the generator's objective \mathcal{L}_ε to be able to minimize it.
- 2) If $f(x + \Delta, y')$ is less than $f(x, y)$ the training algorithm concludes that $\mathcal{L}_\varepsilon(x + \Delta, y)$ has decreased and, consequently, accepts the updates $x + \Delta$ and y' ; otherwise it rejects both updates. We show that after accepting both x and y' , $\mathcal{L}_\varepsilon(x + \Delta, y') < \mathcal{L}_\varepsilon(x, y)$, which implies that our training algorithm does not cycle.
- 3) It then starts the next iteration and proposes a new random update which again depends on its current position.
- 4) While our training algorithm does not cycle, to avoid getting stuck, if it is unable to decrease \mathcal{L}_ε after roughly $\frac{1}{\omega}$ attempts, it concludes w.h.p. that the current x is an approximate local minimum for $\mathcal{L}_\varepsilon(\cdot, y)$ with respect to the given distribution. This is because, by definition, at an approximate local minimum, a random update from the given distribution has probability at most ω of decreasing the generator's objective \mathcal{L}_ε . We also show that the current y is an ε -stationary point for $f(x, \cdot)$.

Remark 2.3 (Choosing the proposal distribution). *In practice, we choose $Q_{x,y}$ to be the stochastic (batch) gradient distribution with mean $-\nabla_x f$. This is motivated by the fact that adding stochastic gradient noise to the steps taken by deep learning algorithms is known empirically to lead to better learning outcomes than adding, e.g., standard Gaussian noise (see e.g., [41]). In our simulations, we observe that this choice of $Q_{x,y}$ leads to GANs which are able to successfully learn*

the distribution of the dataset (Section 4).

Moreover, it can be shown that any update Δ which decreases \mathcal{L}_ε must have a component in the direction of $-\nabla_x f$. To see why this is, note that once the generator proposes an update Δ to x , the discriminator's updates will only increase f , i.e., $\mathcal{L}_\varepsilon(x + \Delta, y) \geq f(x + \Delta, y)$. Moreover, since y is a first-order stationary point of $f(x, \cdot)$ (because y was computed using gradient ascent in the previous iteration), we also have $\mathcal{L}_\varepsilon(x, y) = f(x, y)$. Therefore, we want an update Δ such that

$$f(x + \Delta, y) \leq \mathcal{L}_\varepsilon(x + \Delta, y) \leq \mathcal{L}_\varepsilon(x, y) = f(x, y), \quad (9)$$

which implies that any proposed step which decreases \mathcal{L}_ε must also decrease f (converse is not true).

We conclude this section with a few remarks: 1) While we state Algorithm 1 with stochastic gradients, in practice our training algorithm can be implemented just as easily with ADAM gradients, which we do in our experiments. 2) Algorithm 1 uses a randomized accept-reject rule inspired by simulated annealing— if the resulting loss has decreased, the updates for x and y are accepted; otherwise they are only accepted with a small probability e^{-i/τ_1} at each iteration i , where τ_1 is a “temperature” parameter. 3) While our main result still holds if one replaces simulated annealing with a deterministic acceptance rule, we included the simulated annealing step in Algorithm 1 as it seems to be beneficial in practice in the early period of training when our training algorithm is implemented with ADAM gradients. 4) Finally, in simulations, we find that our training algorithm's implementation can be simplified by taking a small fixed number of discriminator updates at each iteration, instead of taking as many steps as needed to achieve a small gradient.

2.3 Convergence guarantees

Theorem 2.4 (Main result). *Algorithm 1, with hyperparameters $\eta > 0$, $\tau_1 > 0$, given access to stochastic zeroth-order and gradient oracles for a function $f = \sum_{i \in [m]} f_i$ where each f_i is b -bounded with L -Lipschitz gradient for some $b, L > 0$, and $\varepsilon, \delta, \omega > 0$, and an oracle for sampling from a distribution $Q_{x,y}$, with probability at least $9/10$ returns $(x^*, y^*) \in \mathbb{R}^d \times \mathbb{R}^d$ such that, for some $\varepsilon^* \in [\frac{1}{2}\varepsilon, \varepsilon]$, (x^*, y^*) is an approximate local equilibrium (Definition 2.2) w.r.t. $(\varepsilon^*, \delta, \omega)$ and the distribution $Q_{x,y}$. The number of stochastic gradient, function, and sampling oracle calls required by the algorithm is $\text{poly}(b, L, 1/\varepsilon, 1/\delta, 1/\omega)$ and does not depend on the dimension d .*

Theorem 2.4 says that our training algorithm is guaranteed to converge to an approximate local equilibrium for our framework from any starting point, for any f which is bounded with Lipschitz gradients including nonconvex-nonconcave f . As discussed in related work this is in contrast to prior works which assume e.g., that $f(x, y)$ is concave in y or that the training algorithm is provided with an initial point such that the underlying continuous dynamics converge to a local min-max point.

The upper bound assumption on f is satisfied by many loss functions used for training GANs, including the cross-entropy, KL-divergence, and mean-squared-error loss. Although the lower bound assumption is not necessary to prove our results, we include it as it allows us to state our results more concisely. On the other hand, while the smoothness assumption is common in the deep learning literature (e.g., [13]), most neural networks used in practice do not lead to smooth loss functions, and it would be interesting to extend our results to non-smooth f .

We present key ideas in the proof in Section 3, and the full proof in Section 5.

3 Key ideas in the proof

For simplicity, assume $b = L = \tau_1 = 1$ and $\varepsilon = \delta = \omega$. There are two key pieces to proving Theorem 2.4. The first is to show that our algorithm converges to some point (x^*, y^*) in a number of gradient, function, and sampling oracle calls that is $\text{poly}(1/\varepsilon)$ and independent of the dimension d (Lemma 5.5). Secondly, we show that, y^* is a first-order ε -stationary point for $f(x^*, \cdot)$, and x^* is an approximate local minimum of $\mathcal{L}_\varepsilon(\cdot, y^*)$ (Lemma 5.7).

Step 1: Bounding the number of gradient evaluations. After $\Theta(\log(\frac{1}{\varepsilon}))$ steps, the decaying acceptance rate of the simulated annealing step ensures that our algorithm stops whenever $r_{\max} = O(1/\varepsilon)$ proposed steps are rejected in a row. Thus, for every $O(r_{\max})$ iterations where the algorithm does not terminate, with probability at least $1 - \varepsilon$ the value of the loss decreases by more than ε . Since f is 1-bounded, this implies our algorithm terminates after roughly $O(r_{\max}/\varepsilon)$ iterations of the minimization routine (Proposition 5.4).

Next, since f is 1-bounded with 1-Lipschitz gradient, in each iteration, we require at most $\text{poly}(1/\varepsilon)$ gradient ascent steps to reach an ε -stationary point. Since each step of the maximization subroutine requires one gradient evaluation, and each iteration of the minimization routine calls the maximization routine exactly once, the total number of gradient evaluations is $\text{poly}(1/\varepsilon)$.

Step 2: Show x^* is approximate local min for $\mathcal{L}_\varepsilon(\cdot, y^*)$, and y^* is ε -stationary point. First, note that since our algorithm runs the gradient ascent maximization subroutine until it reaches an ε -stationary point, $\|\nabla_y f(x^*, y^*)\| \leq \varepsilon$.

Our stopping condition for the algorithm implies the last r_{\max} updates Δ proposed by the generator were all rejected, and hence were sampled from Q_{x^*, y^*} . Roughly, this implies

$$\Pr_{\Delta \sim Q_{x^*, y^*}} [f(x^* + \Delta, y') \geq f(x^*, y^*) - \varepsilon] \geq 1 - \varepsilon, \quad (10)$$

where the maximization subroutine computes y' by gradient ascent on $f(x^* + \Delta, \cdot)$ initialized at y^* .

To show (7) holds, we need to replace f in the above equation with the generator's objective \mathcal{L}_ε . We first show that the gradient ascent steps form an " ε -increasing" path, starting at y^* with endpoint y' , along which f increases at rate at least ε (Prop. 5.6). Since \mathcal{L}_ε is the supremum of f at the endpoints of *all* such ε -increasing paths starting at y^* ,

$$f(x^* + \Delta, y') \leq \mathcal{L}_\varepsilon(x^* + \Delta, y^*). \quad (11)$$

Finally, recall (Section 2) that $\|\nabla_y f(x^*, y^*)\| \leq \varepsilon^*$ implies

$$\mathcal{L}_\varepsilon(x^*, y^*) = f(x^*, y^*), \quad (12)$$

and hence (8) holds. Finally, plugging (11) and (12) into (10) implies (7) holds.

4 Empirical results

We apply our algorithm to train GANs to learn from both synthetic and real-world datasets. We formulate the GAN using our GAN framework with the cross entropy loss,

$$f(x, y) = -(\log(\mathcal{D}_y(\zeta)) + \log(1 - \mathcal{D}_y(\mathcal{G}_x(\xi)))),$$

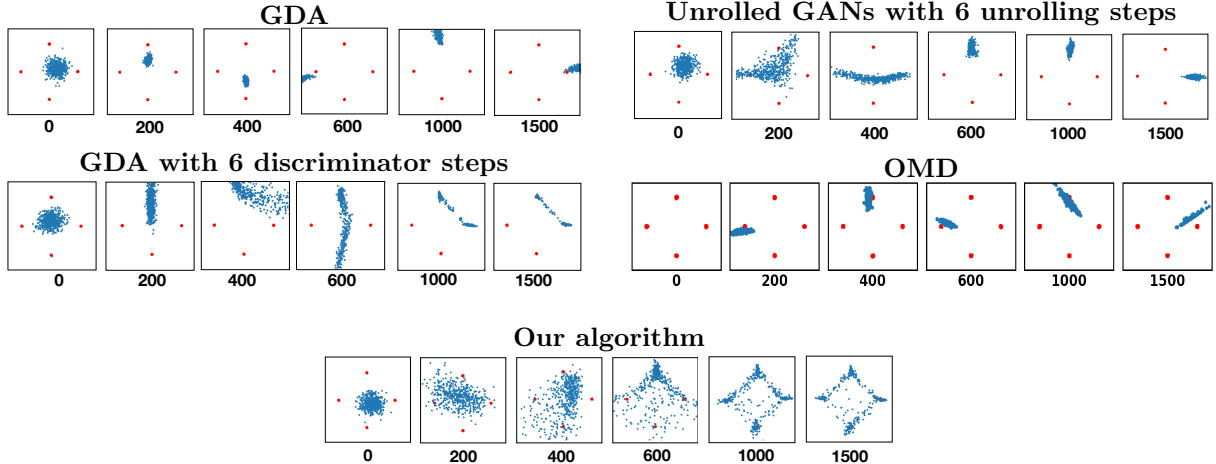


Figure 1: Our algorithm (bottom), unrolled GANs with $k = 6$ unrolling steps (middle), and GDA with $k = 1$ and $k = 6$ discriminator steps (top and second from top) and OMD (second from bottom). Each algorithm was trained on a 4-Gaussian mixture for 1500 iterations. Our algorithm used $k = 6$ discriminator steps and acceptance rate $e^{-1/\tau} = 1/4$. Plots show the points generated by each of these algorithms after the specified number of iterations.

Table 1: Gaussian mixture dataset: The fraction of times (out of 20 repetitions) that each method generates m modes, for $m \in \{1, 2, 3, 4\}$. k represents the number of discriminator steps, per generator step. Our algorithm learns four modes in more repetitions than the other algorithms.

Method	Number of modes learnt			
	1	2	3	4
This paper	0	0.15	0.15	0.70
GDA ($k = 1$)	0.95	0.05	0	0
GDA ($k = 6$)	0.05	0.75	0	0.20
OMD	0.80	0.20	0	0
Unrolled-GAN	0.75	0.15	0.10	0

where x, y are the parameters of the generator and discriminator networks \mathcal{G} and \mathcal{D} respectively, ζ is sampled from the data, and $\xi \sim N(0, I_d)$. ² To adapt Algorithm 1 to training GANs, we make the following simplifications in our simulations:

- 1) *Temperature schedule*. We use a fixed temperature τ , constant with iteration i , making it simpler to choose a good temperature value rather than a temperature schedule.
- 2) *Accept/reject rule*. We replace the randomized acceptance rule with a deterministic rule: If $f_{\text{new}} \leq f_{\text{old}}$ we accept the proposed step, and if $f_{\text{new}} > f_{\text{old}}$ we only accept if i is a multiple of $e^{1/\tau}$ (i.e., an average acceptance rate of $e^{-1/\tau}$).
- 3) *Discriminator steps*. We take a fixed number of discriminator steps at each iteration, instead of taking as many steps needed to achieve a small gradient.

These simplifications do not seem to significantly affect our algorithm's performance (see Appendix D for simulations showing it effectively trains GANs without most of these simplifications).

²Alternatively, one can also use the Wasserstein loss function with our training algorithm.

Moreover, our simulations show that a smaller number of discriminator steps k is sufficient in practice.

Datasets. To illustrate the quality, scalability, and stability of GANs obtained using our training algorithm, we consider a synthetic dataset and real-world datasets.

1) *Gaussian mixture dataset.* This synthetic dataset consists of 512 points sampled from a mixture of four equally weighted Gaussians in two dimensions with standard deviation 0.01 and means at $(0, 1)$, $(1, 0)$, $(-1, 0)$ and $(0, -1)$. Since the modes in this dataset are well-separated, mode collapse, when it occurs, can be clearly detected.

2) *CIFAR-10* [21]. This real-world dataset contains 60K color images from 10 classes. Previous works [5, 27, 39] have noted that it is challenging to detect mode collapse on CIFAR-10, visually or using standard metrics such as Inception Scores, because the modes are not well-separated. We use this dataset primarily to compare the scalability, quality, and stability of GANs in our framework obtained using our training algorithm.

Evaluation metrics. For GANs generated using different training algorithms, we report the final performance and the performance across iterations, where the performance for each dataset is quantified as follows:

- 1) For the Gaussian mixture dataset, we report the number of modes learned by the GAN from each training algorithm.
- 2) For CIFAR-10, we report the Inception Scores [37] at different iterations. Inception Score is a standard heuristic measure for evaluating the quality of CIFAR-10 images and quantifies whether the generated images correspond to specific objects/classes, as well as, whether the GAN generates diverse images. A higher Inception Score is better, and the lowest possible Inception Score is 1.

Baselines. We compare our algorithm’s performance to GDA, Optimistic Mirror Descent (OMD) [9], and unrolled GAN [27]. Note that [9] propose the OMD algorithm for Wasserstein GAN framework; correspondingly, we report the performance of their training algorithm using Wasserstein loss. [27] provide a code implementation of unrolled GANs for toy Gaussian mixture datasets only;³ hence, we compare against their algorithm only for Gaussian mixture dataset. All methods are implemented using ADAM [19] gradients.

Hyperparameters and hardware. The details of the networks and hyperparameter choices are given in Appendix B.1. The simulations are run using four 3.0 GHz Intel Scalable CPUs, provided by AWS, and one High freq. Intel Xeon E5-2686 v4 GPU (for CIFAR-10).

Results. *Gaussian mixture dataset.* We trained GANs on the Gaussian mixture dataset for 1500 iterations using our algorithm, unrolled GANs with 6 unrolling steps, GDA with $k = 1$ and $k = 6$ discriminator steps, and OMD with $k = 6$ discriminator steps. We repeated each simulation 20 times. The performance of the output GAN learned by all training algorithms is presented in Table 1, while Figure 1 also shows the samples from generators of different training algorithm at various iterations. The GAN returned by our training algorithm learns all four modes in 14 (out of 20) repetitions. This is significantly better than other training algorithms, amongst which only

³https://github.com/poolio/unrolled_gan

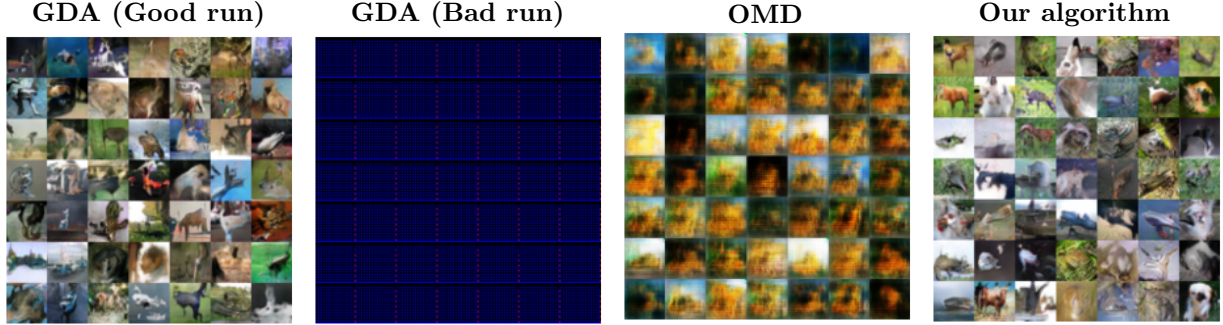


Figure 2: Images generated from GANs trained using GDA (from two different runs), OMD, and our algorithm (with $k = 1$ discriminator steps and acceptance rate $e^{-1/\tau} = 1/2$) on CIFAR-10 for 50,000 iterations; see Appendix B.2 for other results.

Table 2: CIFAR-10 dataset: The mean (and standard error) of Inception Scores of models from different training algorithms. Note that, GDA and our algorithm return generators with similar mean performance; however, the standard error of the Inception Score in case of GDA is relatively larger.

Method	Iteration			
	5000	10000	25000	50000
Ours	2.71 (0.28)	3.57 (0.26)	4.10 (0.35)	4.68 (0.39)
GDA	2.80 (0.52)	3.56 (0.64)	4.28 (0.77)	4.51 (0.86)
OMD	1.60 (0.18)	1.80 (0.37)	1.73 (0.25)	1.96 (0.26)

GDA with $k = 6$ discriminator steps sometimes returns GANs that learn four modes, but only for 4 (out of 20) repetitions. In particular, OMD and unrolled GANs learn at most 2 modes of the dataset, while GDA with $k = 1$ seems to exhibit cycling behaviour in most cases (see Appendix B.2 for images from all runs). Thus, for this synthetic dataset, our algorithm is the most effective in avoiding mode collapse and cycling in comparison to baselines.

CIFAR-10. We ran our algorithm (with $k = 1$ discriminator steps and acceptance rate $e^{-1/\tau} = 1/2$) on CIFAR-10 for 20 repetitions and 50,000 iterations per repetition. We compare with GDA with $k = 1$ discriminator steps and OMD. For all algorithms, we compute the Inception Score every 500 iterations; Table 2 reports the Inception Scores at iteration 5000, 10000, 25000, and 50000, while Figure 3 in the appendix provides the complete plot for Inception Score vs. training iterations. Sample images from all three algorithms are also provided in Figure 2.

The average Inception Score of GANs from both GDA and our algorithm are fairly close to each other, with the final mean Inception Score of 4.68 for our algorithm being somewhat higher than the final mean of 4.51 for GDA. However, the standard error of Inception Scores of GDA is much larger than of our algorithm. The relatively larger standard deviation of GDA is because GDA, in certain runs, does not learn an appropriate distribution at all (Inception Score is close to 1 throughout training in this case), leading to a larger value of standard deviation. Visually, in these GDA runs, the GANs from GDA do not generate recognizable images (Figure 2, second from left).

For all other trials, the images generated by GDA have similar Inception Score (and similar quality) as the images generated by our algorithm. In other words, our algorithm seems to be more stable than GDA and returns GANs that generate high quality images in every repetition (see samples from different trials of GDA and our algorithm in Appendix B.2).

GANs trained using OMD attain much lower Inception Scores than our algorithm.⁴ Moreover, the images generated by GANs trained using OMD have visually much lower quality than the images generated by GANs trained using our algorithm (Figure 2).

Evaluation on CIFAR-10 dataset shows that the GANs from our training algorithm can always generate good quality images; in comparison to OMD, the GANs trained using our algorithm generate higher quality images, while in comparison to GDA, it is relatively more stable.

We evaluate our algorithm on MNIST dataset as well, where it also learns to generate from multiple modes; the results are presented in Appendix C.

Clock time per iteration. When training on CIFAR-10, our algorithm and GDA both took the same amount of time per iteration, 0.08 seconds, on the AWS GPU server.

5 Proof of Theorem 2.4

In this section we give the proof of Theorem 2.4.

Setting parameters: We start by setting parameters which will be used in the proof. Let $b_0 = |B|$, $b_y = |B_y|$ denote the batch sizes. And note that the fact that each f_i has L -Lipschitz gradient for all $i \in [m]$, implies that each f_i is also L_1 -Lipschitz, where $L_1 = \sqrt{2Lb}$.

For the theoretical analysis, we assume $0 < \varepsilon \leq 1$, and set the following parameters:

1. $\nu = \frac{1}{10} \left[\frac{320b(L+1)}{\varepsilon^2} \left(\tau_1 \log\left(\frac{128}{\omega^2}\right) + \frac{2048b}{\omega\delta} \log^2\left(\frac{100}{\omega}(\tau_1 + 1)(8\frac{b}{\delta} + 1)\right) + 1 \right) \right]^{-2}$
2. $r_{\max} = \frac{128}{\omega} \log^2 \left(\frac{100}{\omega}(\tau_1 + 1)(8\frac{b}{\delta} + 1) + \log\left(\frac{1}{\nu}\right) \right)$
3. Define $\mathcal{I} := \tau_1 \log\left(\frac{r_{\max}}{\nu}\right) + 8r_{\max}\frac{b}{\delta} + 1$
4. $\eta = \min\left(\frac{1}{10L}, \frac{1}{8L\mathcal{I}}\right)$
5. Define $\mathcal{J} := \frac{16b}{\eta\varepsilon^2}$
6. $\hat{\varepsilon}_1 = \min(\varepsilon, \eta L, \frac{\delta}{8})$
7. $b_0 = \hat{\varepsilon}_1^{-2} 140^2 b^2 \log(1/\nu)$
8. $b_y = \hat{\varepsilon}_1^{-2} 140^2 L_1^2 \log(1/\nu)$

In particular, we note that $\nu \leq \frac{1}{10} (2\mathcal{J}\mathcal{I} + 2 \times (r_{\max} \frac{2b}{\delta} + 1))^{-1}$, and $r_{\max} \geq \frac{4}{\omega} \log\left(\frac{100\mathcal{I}}{\omega}\right)$. At every iteration $i \leq \mathcal{I}$, where we set $\varepsilon' = \varepsilon_i$. We also have $\varepsilon' \leq \varepsilon_0 \left(\frac{1}{1-2\eta L}\right)^{2i} \leq \varepsilon$.

⁴We could not replicate the performance of OMD reported in [9], even with the implementation provided here - https://github.com/vsyrgkanis/optimistic_GAN_training.

5.1 Step 1: Bounding the number of gradient, function, and sampling oracle evaluations.

The first step in our proof is to bound the number of gradient, function, and sampling oracle evaluations required by our algorithm. Towards this end, we begin by showing a concentration bound (Proposition 5.1) for the value of the stochastic gradient and function oracles used by our algorithm. Next, we bound the number of iterations of its discriminator update subroutine Algorithm 2 (Proposition (16)), and the number of iterations in Algorithm 1 (Proposition 5.4); together, these two bounds imply a $\text{poly}(b, L, 1/\varepsilon, 1/\delta, 1/\omega)$ bound on the number of gradient, function, and sampling oracle evaluations (Lemma 5.5).

Proposition 5.1. *For any $\hat{\varepsilon}_1, \nu > 0$, if we use batch sizes $\mathbf{b}_y = \hat{\varepsilon}_1^{-2} 140^2 L_1^2 \log(1/\nu)$ and $\mathbf{b}_0 = \hat{\varepsilon}_1^{-2} 140^2 b^2 \log(1/\nu)$, we have that*

$$\mathbb{P} \left(\|G_y(x, y) - \nabla_y f(x, y)\| \geq \frac{\hat{\varepsilon}_1}{10} \right) < \nu, \quad (13)$$

and

$$\mathbb{P} \left(|F(x, y) - f(x, y)| \geq \frac{\hat{\varepsilon}_1}{10} \right) < \nu. \quad (14)$$

Proof. From Section 2.2 we have that

$$G_y(x, y) - \nabla_y f(x, y) = \frac{1}{\mathbf{b}_y} \sum_{i \in B_y} [\nabla_y f_i(x, y) - \nabla_y f(x, y)],$$

where the batch $B_y \subseteq [m]$ is sampled iid with replacement from $[m]$.

But since each f_i has L -Lipschitz gradient, we have (with probability 1) that

$$\|\nabla_y f_i(x, y) - \nabla_y f(x, y)\| \leq \|\nabla_y f_i(x, y)\| + \|\nabla_y f(x, y)\| \leq 2L_1.$$

Now,

$$\mathbb{E}[\nabla_y f_i(x, y) - \nabla_y f(x, y)] = \mathbb{E}[\nabla_y f_i(x, y) - \mathbb{E}[\nabla_y f_i(x, y)]] = 0.$$

Therefore, by the Azuma-Hoeffding inequality for mean-zero bounded vectors, we have

$$\mathbb{P} \left(\left\| \frac{1}{\mathbf{b}_y} \sum_{i \in B_y} [\nabla_y f_i(x, y) - \nabla_y f(x, y)] \right\| \geq \frac{s\sqrt{\mathbf{b}_y} + 1}{\mathbf{b}_y} 2L_1 \right) < 2e^{1 - \frac{1}{2}s^2} \quad \forall s > 0.$$

Hence, if we set $s = 6 \log^{1/2}(\frac{2}{\nu})$, we have that $7 \log^{1/2}(\frac{2}{\nu}) \sqrt{\mathbf{b}_y} + 1 \geq s\sqrt{\mathbf{b}_y} + 1$ and hence that

$$\mathbb{P} \left(\left\| \frac{1}{\mathbf{b}_y} \sum_{i \in B_y} [\nabla_y f_i(x, y) - \nabla_y f(x, y)] \right\| \geq \frac{7 \log^{1/2}(\frac{2}{\nu}) \sqrt{\mathbf{b}_y}}{\mathbf{b}_y} 2L_1 \right) < \nu.$$

Therefore,

$$\mathbb{P} \left(\left\| \frac{1}{\mathbf{b}_y} \sum_{i \in B_y} [\nabla_y f_i(x, y) - \nabla_y f(x, y)] \right\| \geq \frac{\hat{\varepsilon}_1}{10} \right) < \nu$$

which completes the proof of Inequality (13).

Inequality (14) follows from the exact same steps as the proof of Inequality (13), if we replace the bound L_1 for $\|\nabla_y f_i(x, y)\|$ with the bound b on $|f_i(x, y)|$. \square

Proposition 5.2. *For every j , with probability at least $1 - \nu$ we have that either $\|G_y(\mathbf{x}, y_j)\| < \varepsilon$, or that*

$$\|\nabla_y f(x_j, y_j) - G_y(\mathbf{x}, y_j)\| \leq \frac{1}{10} \eta L \times \min \left(\|G_y(\mathbf{x}, y_j)\|, \|\nabla_y f(x_j, y_j)\| + \frac{\hat{\varepsilon}_1}{10} \right) \quad (15)$$

and

$$\|y_{j+1} - y_j\| \leq \eta \|G_y(\mathbf{x}, y_j)\| \leq 2\eta \|\nabla_y f(x_j, y_j)\| \quad (16)$$

Proof. By proposition 5.1, we have that, with probability at least $1 - \nu$,

$$\|\nabla_y f(x_j, y_j) - G_y(\mathbf{x}, y_j)\| < \frac{\hat{\varepsilon}_1}{10} \leq \frac{1}{10} \varepsilon \eta L \leq \frac{1}{10} \eta L \times \min \left(\|G_y(\mathbf{x}, y_j)\|, \|\nabla_y f(x_j, y_j)\| + \frac{\hat{\varepsilon}_1}{10} \right),$$

since $\hat{\varepsilon}_1 \leq \min(\varepsilon, \eta L)$. This proves Inequality (15).

Moreover, we have that

$$\|y_{j+1} - y_j\| = \|\eta G_y(\mathbf{x}, y_j)\| \leq \eta (\|\nabla_y f(x_j, y_j)\| + \frac{\hat{\varepsilon}_1}{10})$$

since $\hat{\varepsilon}_1 \leq \varepsilon$ and $\|G_y(\mathbf{x}, y_j)\| \geq \varepsilon$. This proves Inequality (16). \square

Proposition 5.3. *Algorithm 2 terminates in at most $\mathcal{J} := \frac{16b}{\eta \varepsilon^2}$ iterations of its “While” loop, with probability at least $1 - \nu \times \mathcal{J}$.*

Proof. Let $j_{\max} \in \mathbb{N} \cup \{\infty\}$ be the number of iterations of the “While” loop in Algorithm 2.

First, we note that the stopping condition for Algorithm 2 implies that

$$\|G_y(\mathbf{x}, y_j)\| \geq \frac{1}{2} \varepsilon \quad (17)$$

for all $j \leq j_{\max} - 1$.

Since f has L -Lipschitz gradient, there exists a vector u , with $\|u\| \leq L\|y_{j+1} - y_j\|$, such that, for all $j \leq j_{\max} - 1$

$$\begin{aligned} f(y_{j+1}) - f(y_j) &= \langle y_{j+1} - y_j, \nabla_y f(\mathbf{x}, y_j) + u \rangle \\ &= \langle y_{j+1} - y_j, \nabla_y f(\mathbf{x}, y_j) \rangle + \langle y_{j+1} - y_j, u \rangle \\ &= \langle \eta G_y(\mathbf{x}, y_j), G_y(\mathbf{x}, y_j) \rangle - \langle \eta G_y(\mathbf{x}, y_j), G_y(\mathbf{x}, y_j) - \nabla_y f(\mathbf{x}, y_j) \rangle + \langle \eta G_y(\mathbf{x}, y_j), u \rangle \\ &\geq \eta \|G_y(\mathbf{x}, y_j)\|^2 - \eta \|G_y(\mathbf{x}, y_j)\| \times \|G_y(\mathbf{x}, y_j) - \nabla_y f(\mathbf{x}, y_j)\| - \eta \|G_y(\mathbf{x}, y_j)\| \times \|u\| \\ &\stackrel{\text{Prop.5.2}}{\geq} \eta \|G_y(\mathbf{x}, y_j)\|^2 - \eta \|G_y(\mathbf{x}, y_j)\| \times \frac{\eta L}{10} \|G_y(\mathbf{x}, y_j)\| - \eta \|G_y(\mathbf{x}, y_j)\| \times L \|y_{j+1} - y_j\| \\ &= \eta \|G_y(\mathbf{x}, y_j)\|^2 - \frac{1}{10} \eta^2 L \|G_y(\mathbf{x}, y_j)\|^2 - \eta \|G_y(\mathbf{x}, y_j)\| \times L \|\eta G_y(\mathbf{x}, y_j)\| \end{aligned} \quad (18)$$

$$\begin{aligned} &\geq \frac{1}{8} \eta \|G_y(\mathbf{x}, y_j)\|^2 \\ &\stackrel{\text{Eq.17}}{\geq} \frac{1}{2} \eta \varepsilon^2, \end{aligned}$$

with probability at least $1 - \nu$, where the second-to-last inequality holds since $\eta \leq \frac{1}{10L}$.

Since f takes values in $[-b, b]$, Inequality (18) implies that Algorithm 2 terminates in at most $\mathcal{J} := \frac{16b}{\eta \varepsilon^2}$ iterations of its “While” loop, with probability at least $1 - \nu \times \mathcal{J}$. \square

Proposition 5.4. *Algorithm 1 terminates in at most $\mathcal{I} := \tau_1 \log(\frac{r_{\max}}{\nu}) + 8r_{\max} \frac{b}{\delta} + 1$ iterations of its “While” loop, with probability at least $1 - 2\nu \times (r_{\max} \frac{2b}{4\delta} + 1)$.*

Proof. For any $i > 0$, let E_i be the “bad” event that both $f(x_{i+1}, y_{i+1}) - f(x_i, y_i) > -\frac{\delta}{4}$ and $\text{Accept}_i = \text{True}$.

Then by Proposition 5.1, since $\frac{\varepsilon_1}{10} \leq \frac{\delta}{8}$, we have that

$$\mathbb{P}(E_i) \leq e^{-\frac{i}{\tau_1}} + \nu. \quad (19)$$

Define $\hat{\mathcal{I}} := \tau_1 \log(\frac{r_{\max}}{\nu})$.

Then for $i \geq \hat{\mathcal{I}}$, from Line 10 of Algorithm 1 we have by Inequality (19) that

$$\mathbb{P}(E_i) \leq 2\nu.$$

Define $h := r_{\max} \frac{2b}{4\delta} + 1$. Then

$$\mathbb{P}\left(\bigcup_{i=\hat{\mathcal{I}}}^{\hat{\mathcal{I}}+h} E_i\right) \leq 2\nu \times h. \quad (20)$$

Since f takes values in $[-b, b]$, if $\bigcup_{i=\hat{\mathcal{I}}}^{\hat{\mathcal{I}}+h} E_i$ does not occur, the number of accepted steps over the iterations $\hat{\mathcal{I}} \leq i \leq \hat{\mathcal{I}} + h$ (that is, the size of the set $\{i : \hat{\mathcal{I}} \leq i \leq \hat{\mathcal{I}} + h, \text{Accept}_i = \text{True}\}$) is at most $\frac{2b}{4\delta}$.

Therefore, since $h = r_{\max} \frac{2b}{4\delta} + 1$, we must have that there exists a number i , with $\hat{\mathcal{I}} \leq i \leq i + r_{\max} \leq \hat{\mathcal{I}} + h$, such that $\text{Accept}_i = \text{False}$ for all $i \in [i, i + r_{\max}]$.

Therefore the condition in the While loop (Line 2) of Algorithm 1 implies that Algorithm 1 terminates after at most $i + r_{\max} \leq \hat{\mathcal{I}} + h$ iterations of its While loop, as long as $\bigcup_{i=\hat{\mathcal{I}}}^{\hat{\mathcal{I}}+h} E_i$ does not occur.

Therefore, Inequality (20) implies that, with probability at least $1 - 2\nu \times (r_{\max} \frac{2b}{4\delta} + 1)$, Algorithm 1 terminates after at most

$$\hat{\mathcal{I}} + h = \tau_1 \log\left(\frac{r_{\max}}{\nu}\right) + 8r_{\max} \frac{b}{\delta} + 1$$

iterations of its “While” loop. \square

Lemma 5.5. *Algorithm 1 terminates after at most $(\tau_1 \log(\frac{r_{\max}}{\nu}) + 4r_{\max}\frac{b}{\delta} + 1) \times (\mathcal{J} \times \mathfrak{b}_y + \mathfrak{b}_0 + \mathfrak{b}_x)$ gradient, function, and sampling oracle evaluations.*

Proof. Each iteration of the While loop in Algorithm 1 computes one batch gradient with batch size \mathfrak{b}_x , one stochastic function evaluation of batch size \mathfrak{b}_0 , generates one sample from the proposal distribution Q , and calls Algorithm 2 exactly once.

Each iteration of the While loop in Algorithm 2 computes one batch gradient with batch size \mathfrak{b}_y . The result then follows directly from Propositions 5.4 and 5.3. \square

5.2 Step 2: Proving the output (x^*, y^*) of Algorithm 1 is an approximate local equilibrium for our framework.

The second step in our proof is to show that the output of Algorithm 1 is an approximate local equilibrium (Definition 2.2) for our framework with respect to $\varepsilon, \delta, \omega > 0$ and the distribution $Q_{x,y}$ (Lemma 5.7). Towards this end, we first show that the steps taken by the discriminator update subroutine (Algorithm 2) form a path along which the loss f is increasing (Proposition 5.6).

Recall the paths $\gamma(t)$ from Definition 2.1. From now on we will refer to such paths as “ ε -increasing paths”. That is, for any $\varepsilon > 0$, we say that a path $\gamma(t)$ is an “ ε -increasing path” if at every point along this path we have that $\|\frac{d}{dt}\gamma(t)\| = 1$ and that $\frac{d}{dt}f(x, \gamma(t)) \geq \varepsilon$ (Inequality (6)).

Proposition 5.6. *Every time Algorithm 2 is called we have that, with probability at least $1 - 2\nu\mathcal{J}$, the path consisting of the line segments $[y_j, y_{j+1}]$ formed by the points y_j computed by Algorithm 2 has a parametrization $\gamma(t)$ which is an $(1 - 2\eta L)\varepsilon'$ -increasing path.*

Proof. We consider the following continuous unit-speed parametrized path $\gamma(t)$:

$$\gamma(t) = y_j + (t - \sum_{k=1}^{j-1} \|v_k\|) \frac{v_j}{\|v_j\|}, \quad \forall t \in \left[\sum_{k=1}^{j-1} \|v_k\|, \sum_{k=1}^j \|v_k\| \right], \quad j \in [j_{\max}],$$

where $v_j := \eta G_y(x, y_j)$ and j_{\max} is the number of iterations of the While loop of Algorithm 2.

Next, we show that $\frac{d}{dt}f(x, \gamma(t)) \geq \varepsilon'$. For each $j \in [j_{\max}]$ we have that

$$\begin{aligned} \frac{d}{dt}f(x, \gamma(t)) &\geq [\nabla_y f(x, y_j) - L\|y_{j+1} - y_j\|u]^\top \frac{v_j}{\|v_j\|} \\ &= [\nabla_y f(x, y_j) - L\eta\|G_y(x, y_j)\|u]^\top \frac{v_j}{\|v_j\|} \\ &\stackrel{\text{Prop.5.1}}{\geq} \left[G_y(x, y_j) - \frac{1}{10}\eta L\|G_y(x, y_j)\|w - L\eta\|G_y(x, y_j)\|u \right]^\top \frac{G_y(x, y_j)}{\|G_y(x, y_j)\|} \\ &\geq \|G_y(x, y_j)\| - \frac{1}{10}\eta L\|G_y(x, y_j)\| - L\eta\|G_y(x, y_j)\| \\ &\geq (1 - 2\eta L)\|G_y(x, y_j)\| \\ &\geq (1 - 2\eta L)\varepsilon' \quad \forall t \in \left[\sum_{k=1}^{j-1} \|v_k\|, \sum_{k=1}^j \|v_k\| \right], \end{aligned} \tag{21}$$

with probability at least $1 - \nu$ for some unit vectors $u, w \in \mathbb{R}^d$.

But by Proposition 5.3 we have that $j_{\max} \leq \mathcal{J}$ with probability at least $1 - \nu \times \mathcal{J}$. Therefore inequality (21) implies that

$$\frac{d}{dt} f(\mathbf{x}, \gamma(t)) \geq (1 - 2\eta L)\varepsilon' \quad \forall t \in [0, \sum_{k=1}^{j_{\max}} \|v_k\|],$$

with probability at least $1 - 2\nu\mathcal{J}$. \square

Lemma 5.7. *Let i^* be such that $i^* - 1$ is the last iteration i of the “While” loop in Algorithm 1 for which $\text{Accept}_i = \text{True}$. Then with probability at least $1 - 2\nu\mathcal{J}\mathcal{I} - 2\nu \times (r_{\max} \frac{2b}{\delta} + 1)$ we have that*

$$\|\nabla_y f(x^*, y^*)\| \leq (1 - \eta L)\varepsilon_{i^*}. \quad (22)$$

Moreover, with probability at least $1 - \frac{\omega}{100} - 2\nu \times (r_{\max} \frac{2b}{\delta} + 1)$ we have that

$$\begin{aligned} & \mathbb{P}_{\Delta \sim Q_{x^*, y^*}} \left(\mathcal{L}_{\varepsilon_{i^*}}(x^* + \Delta, y^*) \right. \\ & \leq \mathcal{L}_{\varepsilon_{i^*}}(x^*, y^*) - \frac{1}{2}\delta \left| x^*, y^* \right. \leq \frac{1}{2}\omega. \end{aligned} \quad (23)$$

and that

$$\frac{\varepsilon}{2} \leq \varepsilon_{i^*} \leq \varepsilon. \quad (24)$$

Proof. First, we note that $(x^*, y^*) = (x_i, y_i)$ for all $i \in \{i^*, \dots, i^* + r_{\max}\}$, and that Algorithm 1 stops after exactly $i^* + r_{\max}$ iterations of the “While” loop in Algorithm 1.

Let H_i be the “bad” event that, when Algorithm 2 is called during the i th iteration of the “While” loop in Algorithm 1, the path traced by Algorithm 2 is not an ε_i -increasing path. Then, by Proposition 5.6 we have that

$$\mathbb{P}(\mathsf{H}_i) \leq 2\nu\mathcal{J}. \quad (25)$$

Let K_i be the “bad” event that $\|G_y(x_i, y_i) - \nabla_y f(x_i, y_i)\| \geq \frac{\hat{\varepsilon}_1}{10}$. Then by Propositions 5.1 and 5.3 we have that

$$\mathbb{P}(\mathsf{K}_i) \leq 2\nu\mathcal{J}. \quad (26)$$

Whenever K_i^c occurs we have that

$$\begin{aligned} \|\nabla_y f(x_i, y_i)\| & \leq \|G_y(x_i, y_i)\| + \|G_y(x_i, y_i) - \nabla_y f(x_i, y_i)\| \\ & \leq (1 - 2\eta L)\varepsilon_i + \|G_y(x_i, y_i) - \nabla_y f(x_i, y_i)\| \\ & \leq (1 - 2\eta L)\varepsilon_i + \frac{\hat{\varepsilon}_1}{10} \\ & \leq (1 - \eta L)\varepsilon_i, \end{aligned} \quad (27)$$

where the second Inequality holds by Line 4 of Algorithm 2, and the last inequality holds since $\frac{\hat{\varepsilon}_1}{10} \leq \eta L$.

Therefore, Inequalities (26) and (27) together with Proposition 5.4 imply that

$$\|\nabla_y f(x^*, y^*)\| \leq (1 - \eta L)\varepsilon_{i^*}$$

with probability at least $1 - 2\nu\mathcal{J}\mathcal{I} - 2\nu \times (r_{\max} \frac{2b}{4\delta} + 1)$. This proves Inequality (22).

Inequality (27) also implies that, whenever K_i^c occurs, the set $P_{\varepsilon_i}(x_i, y_i)$ of endpoints of ε_i -increasing paths with initial point y_i (and x -value x_i) consists only of the single point y_i . Therefore, we have that

$$\mathcal{L}_{\varepsilon_i}(x_i, y_i) = f(x_i, y_i) \quad (28)$$

whenever K_i^c occurs.

Moreover, whenever H_i^c occurs we have that \mathcal{Y}_{i+1} is the endpoint of an ε_i -increasing path with starting point $(x_i + \Delta_i, y_i)$. Now, $\mathcal{L}_{\varepsilon_i}(x_i + \Delta_i, y_i)$ is the supremum of the value of f at the endpoints of all ε_i -increasing paths with starting point $(x_i + \Delta_i, y_i)$. Therefore, we must have that

$$\mathcal{L}_{\varepsilon_i}(x_i + \Delta_i, y_i) \geq f(x_i + \Delta_i, \mathcal{Y}_{i+1}) \quad (29)$$

whenever H_i^c occurs.

Therefore,

$$\begin{aligned} & \mathbb{P}_{\Delta \sim Q_{x_i, y_i}} \left(\mathcal{L}_{\varepsilon_i}(x_i + \Delta, y_i) > \mathcal{L}_{\varepsilon_i}(x_i, y_i) - \frac{1}{2}\delta \middle| x_i, y_i \right) \\ & \stackrel{\text{Eq.28,29}}{\geq} \mathbb{P}_{\Delta \sim Q_{x_i, y_i}} \left(f(x_i + \Delta, \mathcal{Y}_{i+1}) > f(x_i, y_i) - \frac{1}{2}\delta \middle| x_i, y_i \right) - \mathbb{P}(\mathsf{H}_i) - \mathbb{P}(\mathsf{K}_i) \\ & \stackrel{\text{Prop.5.1}}{\geq} \mathbb{P}_{\Delta \sim Q_{x_i, y_i}} \left(F(x_i + \Delta, \mathcal{Y}_{i+1}) > F(x_i, y_i) - \frac{1}{4}\delta \middle| x_i, y_i \right) - 2\nu - \mathbb{P}(\mathsf{H}_i) - \mathbb{P}(\mathsf{K}_i) \\ & \geq \mathbb{P} \left(\text{Accept}_i = \text{False} \middle| x_i, y_i \right) - 2\nu - \mathbb{P}(\mathsf{H}_i) - \mathbb{P}(\mathsf{K}_i) \\ & \stackrel{\text{Eq.25,26}}{\geq} \mathbb{P} \left(\text{Accept}_i = \text{False} \middle| x_i, y_i \right) - 2\nu - 2\nu\mathcal{J} - 2\nu\mathcal{I}, \quad \forall i \leq \mathcal{I}, \end{aligned} \quad (30)$$

where the second inequality holds by Proposition 5.1, since $\frac{\hat{\varepsilon}_1}{10} \leq \frac{\delta}{8}$.

Define

$$p_i := \mathbb{P}_{\Delta \sim Q_{x_i, y_i}} \left(\mathcal{L}_{\varepsilon_i}(x_i + \Delta, y_i) > \mathcal{L}_{\varepsilon_i}(x_i, y_i) - \frac{1}{2}\delta \middle| x_i, y_i \right)$$

for every $i \in \mathbb{N}$. Then Inequality (30) implies that

$$\mathbb{P}(\text{Accept}_i = \text{False} \mid x_i, y_i) \leq p_i + \nu(4\mathcal{J} + 2) \leq p_i + \frac{1}{8}\omega \quad \forall i \leq \mathcal{I}, \quad (31)$$

since $\nu \leq \frac{\omega}{32\mathcal{J} + 16}$.

We now consider what happens for indices i for which $p_i \leq 1 - \frac{1}{2}\omega$. Since $(x_{i+s}, y_{i+s}) = (x_i, y_i)$ whenever $\text{Accept}_{i+k} = \text{False}$ for all $0 \leq k \leq s$, we have by Inequality (31) that

$$\mathbb{P} \left(\bigcap_{s=0}^{r_{\max}} \{\text{Accept}_{i+s} = \text{False}\} \middle| p_i \leq 1 - \frac{1}{2}\omega \right) \leq (1 - \frac{1}{4}\omega)^{r_{\max}} \leq \frac{\omega}{100\mathcal{I}} \quad \forall i \leq \mathcal{I} - r_{\max}$$

since $r_{\max} \geq \frac{4}{\omega} \log(\frac{100\mathcal{I}}{\omega})$.

Therefore, with probability at least $1 - \frac{\omega}{100\mathcal{I}} \times \mathcal{I} = 1 - \frac{\omega}{100}$, we have that the event $\cap_{s=0}^{r_{\max}} \{\text{Accept}_{i+s} = \text{False}\}$ does not occur for any $i \leq \mathcal{I} - r_{\max}$ for which $p_i \leq 1 - \frac{1}{2}\omega$.

Recall from Proposition 5.4 that Algorithm 1 terminates in at most \mathcal{I} iterations of its “While” loop, with probability at least $1 - 2\nu \times (r_{\max} \frac{2b}{4\delta} + 1)$.

Therefore,

$$\mathbb{P}\left(p_{i^*} > 1 - \frac{1}{2}\omega\right) \geq 1 - \frac{\omega}{100} - 2\nu \times \left(r_{\max} \frac{2b}{4\delta} + 1\right). \quad (32)$$

In other words, by the definition of p_{i^*} , Inequality (32) implies that with probability at least $1 - \frac{\omega}{100} - 2\nu \times (r_{\max} \frac{2b}{4\delta} + 1)$, the point (x^*, y^*) is such that

$$\mathbb{P}_{\Delta \sim Q_{x^*, y^*}} \left(\mathcal{L}_{\varepsilon_{i^*}}(x^* + \Delta, y^*) \leq \mathcal{L}_{\varepsilon_{i^*}}(x^*, y^*) - \frac{1}{2}\delta \middle| x^*, y^* \right) \leq \frac{1}{2}\omega.$$

This completes the proof of inequality (23).

Finally we note that when Algorithm 1 terminates in at most \mathcal{I} iterations of its “While” loop, we have

$$\varepsilon_{i^*} = \varepsilon_0 \left(\frac{1}{1 - 2\eta L} \right)^{2i^*} \leq \varepsilon_0 \left(\frac{1}{1 - 2\eta L} \right)^{2\mathcal{I}} \leq \varepsilon, \quad (33)$$

since $\eta \leq \frac{1}{8L\mathcal{I}}$. This completes the proof of Inequality (24). \square

We can now complete the proof of the main theorem:

Proof of Theorem 2.4. First, by Lemma 5.5 our algorithm converges to some point (x^*, y^*) after at most $(\tau_1 \log(\frac{r_{\max}}{\nu}) + 4r_{\max} \frac{b}{\delta} + 1) \times (\mathcal{J} \times \mathfrak{b}_y + \mathfrak{b}_0 + \mathfrak{b}_x)$ gradient, function, and sampling oracle evaluations, which is polynomial in $b, L_1, L, 1/\varepsilon, 1/\delta, 1/\omega$, and does not depend on the dimension d .

By Lemma 5.7, if we set $\varepsilon^* = \varepsilon_{i^*}$, we have that Inequalities (8) and (7) hold for parameters $\varepsilon^* \in [\frac{1}{2}\varepsilon, \varepsilon]$, δ, ω and distribution Q , with probability at least $1 - 2\nu\mathcal{J}\mathcal{I} - 2\nu \times (r_{\max} \frac{2b}{4\delta} + 1) \geq \frac{9}{10}$, since $\nu \leq \frac{1}{10}(2\mathcal{J}\mathcal{I} + 2 \times (r_{\max} \frac{2b}{4\delta} + 1))^{-1}$. \square

6 Conclusion and future directions

In this paper, we show how a greedy first-order variant of the classic min-max GAN framework can be used to obtain novel algorithms for training GANs geared towards learning distributions over images. Our algorithm comes with efficiency and convergence guarantees for nonconvex-nonconcave loss functions. Importantly, GANs trained using a version of our algorithm show improved stability on synthetic and real-world datasets.

While we show that our algorithm runs in time polynomial in b, L , and independent of the dimension d , we do not believe our bounds are tight and it would be interesting to show that our algorithm runs in time that is linear in b, L .

While our theoretical guarantees (Theorem 2.4) hold for any distribution Q , we implement our training algorithm using the distribution of ADAM stochastic gradients rather than, e.g., a standard Gaussian as this leads to better performance in practice. It would be interesting to see if a

specialized analysis of our algorithm geared towards adaptively preconditioned distributions can lead to improved bounds.

Finally, while we explored image generation in this paper, it would be interesting to find applications of our GAN framework and the training algorithm to other domains where min-max GANs have been deployed.

Acknowledgments

This research was supported in part by NSF CCF-1908347 grant and an AWS ML research award.

References

- [1] Naman Agarwal, Zeyuan Allen-Zhu, Brian Bullins, Elad Hazan, and Tengyu Ma. Finding approximate local minima faster than gradient descent. In *Proceedings of the 49th Annual ACM SIGACT Symposium on Theory of Computing*, pages 1195–1199, 2017.
- [2] Martín Arjovsky and Léon Bottou. Towards principled methods for training generative adversarial networks. In *5th International Conference on Learning Representations, ICLR 2017, Toulon, France, April 24-26, 2017, Conference Track Proceedings*, 2017.
- [3] Martin Arjovsky, Soumith Chintala, and Léon Bottou. Wasserstein generative adversarial networks. In *International conference on machine learning*, pages 214–223, 2017.
- [4] Rowel Atienza. GAN by example using keras on tensorflow backend. “<https://towardsdatascience.com/gan-by-example-using-keras-on-tensorflow-backend-1a6d515a60d0>”, 2017.
- [5] Ali Borji. Pros and cons of GAN evaluation measures. *Computer Vision and Image Understanding*, 179:41–65, 2019.
- [6] Jason Brownlee. How to develop a GAN to generate CIFAR10 small color photographs. “<https://machinelearningmastery.com/how-to-develop-a-generative-adversarial-network-for-a-cifar-10-small-object-photographs-from-scratch/>”, 2019.
- [7] Sébastien Bubeck. Convex optimization: Algorithms and complexity. *Foundations and Trends in Machine Learning*, 8, 2017.
- [8] Tong Che, Yanran Li, Athul Paul Jacob, Yoshua Bengio, and Wenjie Li. Mode regularized generative adversarial networks. In *International Conference on Learning Representations, ICLR*, 2017.
- [9] Constantinos Daskalakis, Andrew Ilyas, Vasilis Syrgkanis, and Haoyang Zeng. Training GANs with optimism. In *International Conference on Learning Representations*, 2018.
- [10] Constantinos Daskalakis and Ioannis Panageas. The limit points of (optimistic) gradient descent in min-max optimization. In S. Bengio, H. Wallach, H. Larochelle, K. Grauman, N. Cesa-Bianchi, and R. Garnett, editors, *Advances in Neural Information Processing Systems 31*, pages 9236–9246. Curran Associates, Inc., 2018.

- [11] Vincent Dumoulin, Ishmael Belghazi, Ben Poole, Alex Lamb, Martín Arjovsky, Olivier Mastropietro, and Aaron C. Courville. Adversarially learned inference. In *5th International Conference on Learning Representations, ICLR 2017, Toulon, France, April 24-26, 2017, Conference Track Proceedings*, 2017.
- [12] Maayan Frid-Adar, Eyal Klang, Michal Amitai, Jacob Goldberger, and Hayit Greenspan. Synthetic data augmentation using GAN for improved liver lesion classification. In *2018 IEEE 15th international symposium on biomedical imaging (ISBI 2018)*, pages 289–293. IEEE, 2018.
- [13] Rong Ge, Furong Huang, Chi Jin, and Yang Yuan. Escaping from saddle points—online stochastic gradient for tensor decomposition. In *Conference on Learning Theory*, pages 797–842, 2015.
- [14] Ian Goodfellow, Jean Pouget-Abadie, Mehdi Mirza, Bing Xu, David Warde-Farley, Sherjil Ozair, Aaron Courville, and Yoshua Bengio. Generative adversarial nets. In *Advances in neural information processing systems*, pages 2672–2680, 2014.
- [15] Ishaan Gulrajani, Faruk Ahmed, Martin Arjovsky, Vincent Dumoulin, and Aaron C Courville. Improved training of Wasserstein GANs. In *Advances in neural information processing systems*, pages 5767–5777, 2017.
- [16] Martin Heusel, Hubert Ramsauer, Thomas Unterthiner, Bernhard Nessler, and Sepp Hochreiter. GANs trained by a two time-scale update rule converge to a local Nash equilibrium. In *Advances in Neural Information Processing Systems*, pages 6626–6637, 2017.
- [17] Chi Jin, Praneeth Netrapalli, and Michael I. Jordan. What is local optimality in nonconvex–nonconcave minimax optimization? In *ICML 2020*. International Machine Learning Society (IMLS), 2020.
- [18] Renu Khandelwal. Generative adversarial network (GAN) using keras. “<https://medium.com/datadriveninvestor/generative-adversarial-network-gan-using-keras-ce1c05cfdf3>”, 2019.
- [19] Diederik P. Kingma and Jimmy Ba. Adam: A method for stochastic optimization. In *International Conference for Learning Representations*, pages 1595–1625, 2015.
- [20] Diederik P Kingma, Danilo J Rezende, Shakir Mohamed, and Max Welling. Semi-supervised learning with deep generative models. In *Proceedings of the 27th International Conference on Neural Information Processing Systems-Volume 2*, pages 3581–3589, 2014.
- [21] Alex Krizhevsky, Vinod Nair, and Geoffrey Hinton. CIFAR-10 (Canadian Institute for Advanced Research). 2009.
- [22] Yann LeCun, Corinna Cortes, and CJ Burges. MNIST handwritten digit database. *ATT Labs [Online]. Available: <http://yann.lecun.com/exdb/mnist>*, 2, 2010.
- [23] Songtao Lu, Ioannis Tsaknakis, Mingyi Hong, and Yongxin Chen. Hybrid block successive approximation for one-sided non-convex min-max problems: algorithms and applications. *IEEE Transactions on Signal Processing*, 2020.

[24] Oren Mangoubi and Nisheeth K. Vishnoi. Greedy adversarial equilibrium: An efficient alternative to nonconvex-nonconcave min-max optimization. In *ACM Symposium on Theory of Computing (STOC)*, 2021.

[25] Panayotis Mertikopoulos, Bruno Lecouat, Houssam Zenati, Chuan-Sheng Foo, Vijay Chandrasekhar, and Georgios Piliouras. Optimistic mirror descent in saddle-point problems: Going the extra (gradient) mile. In *International Conference on Learning Representations (ICLR 2019)*, 2019.

[26] Lars Mescheder, Sebastian Nowozin, and Andreas Geiger. The numerics of GANs. In *Advances in Neural Information Processing Systems*, pages 1825–1835, 2017.

[27] Luke Metz, Ben Poole, David Pfau, and Jascha Sohl-Dickstein. Unrolled generative adversarial networks. In *5th International Conference on Learning Representations, ICLR 2017, Toulon, France, April 24-26, 2017, Conference Track Proceedings*, 2017.

[28] Takeru Miyato, Toshiki Kataoka, Masanori Koyama, and Yuichi Yoshida. Spectral normalization for generative adversarial networks. In *International Conference on Learning Representations*, 2018.

[29] Aryan Mokhtari, Asuman Ozdaglar, and Sarath Pattathil. A unified analysis of extra-gradient and optimistic gradient methods for saddle point problems: Proximal point approach. In *International Conference on Artificial Intelligence and Statistics*, pages 1497–1507. PMLR, 2020.

[30] Sudipto Mukherjee, Himanshu Asnani, Eugene Lin, and Sreeram Kannan. Clustergan: Latent space clustering in generative adversarial networks. In *Proceedings of the AAAI conference on artificial intelligence*, volume 33, pages 4610–4617, 2019.

[31] Vaishnavh Nagarajan and J Zico Kolter. Gradient descent GAN optimization is locally stable. In *Advances in Neural Information Processing Systems*, pages 5585–5595, 2017.

[32] Arkadi Nemirovski. Prox-method with rate of convergence $O(1/T)$ for variational inequalities with Lipschitz continuous monotone operators and smooth convex-concave saddle point problems. *SIAM Journal on Optimization*, 15(1):229–251, 2004.

[33] Yurii Nesterov and Boris T Polyak. Cubic regularization of Newton method and its global performance. *Mathematical Programming*, 108(1):177–205, 2006.

[34] Thu Nguyen-Phuoc, Chuan Li, Lucas Theis, Christian Richardt, and Yong-Liang Yang. Hologan: Unsupervised learning of 3d representations from natural images. In *Proceedings of the IEEE/CVF International Conference on Computer Vision*, pages 7588–7597, 2019.

[35] Alexander Rakhlin and Karthik Sridharan. Online learning with predictable sequences. In *Conference on Learning Theory*, pages 993–1019. PMLR, 2013.

[36] Tim Salimans, Ian J Goodfellow, Wojciech Zaremba, Vicki Cheung, Alec Radford, and Xi Chen. Improved techniques for training GANs. In *NeurIPS Deep Learning Symposium*, 2016.

[37] Tim Salimans, Han Zhang, Alec Radford, and Dimitris Metaxas. Improving GANs using optimal transport. In *International Conference on Learning Representations*, 2018.

- [38] Shibani Santurkar, Ludwig Schmidt, and Aleksander Madry. A classification-based study of covariate shift in GAN distributions. In *International Conference on Machine Learning*, pages 4480–4489. PMLR, 2018.
- [39] Akash Srivastava, Lazar Valkov, Chris Russell, Michael U Gutmann, and Charles Sutton. Veegan: Reducing mode collapse in GANs using implicit variational learning. In *Advances in Neural Information Processing Systems*, pages 3308–3318, 2017.
- [40] Nisheeth K. Vishnoi. *Algorithms for Convex Optimization*. Cambridge University Press, 2021.
- [41] Zhanxing Zhu, Jingfeng Wu, Bing Yu, Lei Wu, and Jinwen Ma. The anisotropic noise in stochastic gradient descent: Its behavior of escaping from sharp minima and regularization effects. In *ICML*, pages 7654–7663, 2019.

A Extension to functions with compact convex support

In this section we introduce a version of our training algorithm (Section A.1) for loss functions with compact convex support, and run it on a simple bilinear loss function (Section A.2). We then show that, if f is also convex-concave, then, for $\varepsilon = \delta = \omega = 0$, an approximate local equilibrium for our framework is equivalent to a global min-max point (Section A.3).

A.1 Projected gradient algorithm for compactly supported loss

Our training algorithm can be easily extended to the setting of functions $f : \mathcal{X} \times \mathcal{Y} \rightarrow \mathbb{R}$ where $\mathcal{X} \subseteq \mathbb{R}^d$ and $\mathcal{Y} \subseteq \mathbb{R}^d$ are compact convex sets, by replacing the stochastic gradient update $y - \eta G_y(x, y)$ in Algorithm 1 with a projected gradient update $\mathcal{P}_{\mathcal{Y}}(y - \eta G_y(x, y))$ (Algorithm 3), if one has access to a projection oracle $\mathcal{P}_{\mathcal{Y}}$ for the set \mathcal{Y} . (In other words, for any point $z \in \mathbb{R}^d$, $\mathcal{P}_{\mathcal{Y}}(z) = \operatorname{argmin}_{w \in \mathcal{Y}} \|w - z\|$ is the projection of z onto the set \mathcal{Y} .)

When choosing a proposal distribution $Q_{x,y}$ for the proposed generator updates in Algorithm 3, one must be careful to make sure that each sample $\Delta \sim Q_{x,y}$ from this distribution is such that $x + \Delta \in \mathcal{X}$. For instance, given access to a projection oracle $\mathcal{P}_{\mathcal{X}}$ for the compact convex set \mathcal{X} , one may choose $Q_{x,y}$ to be the distribution such that the proposed updates $\Delta \sim Q_{x,y}$ are $\Delta = \mathcal{P}_{\mathcal{X}}(x + \xi) - x$, where $\xi \sim N(0, I_d)$. Alternatively, one may choose the distribution of proposed updates $\Delta \sim Q_{x,y}$ to be such that $\Delta = \mathcal{P}_{\mathcal{X}}(x - \eta G_x(x, y)) - x$, where G_x is a stochastic gradient with mean $\nabla_x f(x, y)$ and $\eta > 0$.

A.2 Simple application to bi-linear losses

As a simple application of Algorithm 3, consider the bilinear loss function $f(x, y) = xy$ where x and y are constrained to the set $[-\frac{1}{2}, \frac{1}{2}]$. It is easy to see that the set of global min-max points consists of the points (x, y) where $x = 0$ and y is any point in $[-\frac{1}{2}, \frac{1}{2}]$. The approximate local equilibria for our framework (with $\varepsilon = \delta > 0$, $\omega = 0$, and e.g. proposal distribution $\Delta \sim Q_{x,y}$ with $\Delta = \mathcal{P}_{\mathcal{X}}(x + \xi) - x$, where $\xi \sim N(0, 1)$) are the set of points (x, y) where x is any point in $[-\varepsilon, \varepsilon]$ and y is any point in $[-\frac{1}{2}, \frac{1}{2}]$.

This is because, when running Algorithm 3 on this example, if x is outside the set $[-\varepsilon, \varepsilon]$, the discriminator will follow an increasing trajectory to always return a point $y = -\frac{1}{2}$ or $y = \frac{1}{2}$, which means that, roughly speaking, the generator is attempting to minimize the function $\frac{1}{2}|x|$. This means that the algorithm will accept all updates $x + \Delta$ for which $\frac{1}{2}|x + \Delta| < \frac{1}{2}|x| - \frac{\varepsilon}{2}$, implying that the algorithm converges towards a point with $|x| \leq \varepsilon$.

Thus, as ε goes to zero, the set of approximate local equilibria for our framework coincides with the set of global min-max optima for the function $f(x, y) = xy$.

This latter fact holds more generally for any convex-concave function with compact convex domain (see Theorem A.1).

Experiments on compactly supported bi-linear loss. Next, we discuss numerical simulations on the bilinear loss function $f(x, y) = xy$ with compact support $(x, y) \in [-1, 1] \times [-1, 1]$. For this function, the gradient descent-ascent algorithm is known to diverge away from the global min-max point (see for instance [17]).

Algorithm 3 Training algorithm for compactly supported loss

input: A stochastic zeroth-order oracle F for loss function $f : \mathcal{X} \times \mathcal{Y} \rightarrow \mathbb{R}$ where $\mathcal{X}, \mathcal{Y} \subseteq \mathbb{R}^d$ are compact convex sets. Stochastic gradient oracle G_y with mean $\nabla_y f$, and sampling oracle for a distribution $Q_{x,y}$ where $\Delta \sim Q_{x,y}$ is such that $x + \Delta \in \mathcal{X}$. Projection oracle $\mathcal{P}_y : \mathbb{R}^d \rightarrow \mathcal{Y}$ for \mathcal{Y} . An initial point $(x, y) \in \mathcal{X} \times \mathcal{Y}$, and parameters $\varepsilon, \delta, \omega$.

output: A point (x^*, y^*)

hyperparameters: r_{\max} (maximum number of rejections), $\eta > 0$.

```

Set  $r \leftarrow 0, i \leftarrow 0$ 
while  $r \leq r_{\max}$  do
   $f_{\text{old}} \leftarrow F(x, y)$ ,
  Sample  $\Delta \sim Q_{x,y}$  {Sample proposed generator update from the given distribution Q}
  Set  $x' \leftarrow x + \Delta$  {Compute the proposed update for the generator}
  Set  $j \leftarrow 0$ 
  Set  $y \leftarrow y$  and Stop = False
  while Stop = False do
    Set  $j \leftarrow j + 1$ 
    Set  $g_{y,j} \leftarrow G_y(x, y_j)$ 
    if  $\frac{1}{\eta} \|y - \mathcal{P}_y(y - \eta g_{y,j})\| > \varepsilon'$  then
      Set  $y \leftarrow \mathcal{P}_y(y - \eta g_{y,j})$  {Compute discriminator's update via gradient ascent}
    else
      Set Stop = True
    Set  $f_{\text{new}} \leftarrow F(x', y')$  {Compute the new loss value}
    Set Accept  $\leftarrow$  True.
    if  $f_{\text{new}} > f_{\text{old}} - \delta/2$ , set Accept  $\leftarrow$  False {accept or reject}
    if Accept = True then Set  $x \leftarrow x', y \leftarrow y', r \leftarrow 0$  {Accept the updates}
    else Set  $r \leftarrow r + 1$  {Reject the updates, and track how many successive steps were rejected.}
    Set  $i \leftarrow i + 1$ 
return  $(x, y)$ 

```

This function has global min-max point at every point in the set $\{(x, y) : x = 0, y \in [-1, 1]\}$. We ran Algorithm 3 on this function with hyperparameters $\eta = 0.2$, $\varepsilon = \delta = 0.06$, and $r_{\max} = 5$, value oracle $F(x, y) = f(x, y)$, gradient oracle $G_y(x, y) = \nabla_y f(x, y)$, and initial point $(x, y) = (0.4, 0.4)$. Our choice of distribution $Q_{x,y}$ for the proposed updates $\Delta \sim Q_{x,y}$ is such that $\Delta = \mathcal{P}_{\mathcal{X}}(\nabla_x f(x, y) + \xi) - x$, where $\xi \sim N(0, 1)$ and $\mathcal{P}_{\mathcal{X}}$ is a projection oracle for the set $\mathcal{X} = [-1, 1]$. After 341 iterations of the outer loop, our algorithm reached the point $(0.0279, -0.9944)$, which is very close to one of its true global min-max points, $(0, -1)$.

A.3 Comparison of local equilibrium and global min-max in the compactly supported convex-concave setting.

In the following we assume that $f : \mathcal{X} \times \mathcal{Y} \rightarrow \mathbb{R}$, where $\mathcal{X}, \mathcal{Y} \subset \mathbb{R}^d$ are two compact convex sets, and that f is continuously differentiable on $\mathcal{X} \times \mathcal{Y}$. We denote by $\nabla_y^{\mathcal{Y}}$ the projected gradient in the y variable for the set \mathcal{Y} .

The following theorem shows that, in the compactly supported convex-concave setting, a point (x^*, y^*) is an approximate local equilibrium for our framework (for $\varepsilon = \delta = \omega = 0$) if and only if it is a global min-max point:

Theorem A.1. *Let $f : \mathcal{X} \times \mathcal{Y} \rightarrow \mathbb{R}$ be convex-concave, where $\mathcal{X}, \mathcal{Y} \subseteq \mathbb{R}^d$ are compact convex sets. And let $Q_{x,y}$ be a continuous distribution with support on \mathcal{X} such that, for every $(x, y) \in \mathcal{X} \times \mathcal{Y}$, there is some open ball $B \subset \mathbb{R}^d$ containing x such that $Q_{x,y}$ has non-zero probability density at every point in $B \cap \mathcal{Y}$. Then (x^*, y^*) is an approximate local equilibrium for our framework, with respect to $\varepsilon = \omega = \delta = 0$ and the given distribution $Q_{x,y}$, if and only if it is a global min-max point.*

Proof. Define the “global max” function $\psi(x) := \max_{y \in \mathcal{Y}} f(x, y)$ for all $x \in \mathcal{X}$. We start by showing that the function $\psi(x)$ is convex on the convex set \mathcal{X} . Indeed, for any $x_1, x_2 \in \mathcal{X}$ and any $\lambda \in [0, 1]$ we have

$$\begin{aligned} \lambda\psi(\lambda x_1 + (1 - \lambda)x_2) &= \max_{y \in \mathcal{Y}} f(\lambda x_1 + (1 - \lambda)x_2, y) \\ &\leq \max_{y \in \mathcal{Y}} [\lambda f(x_1, y) + (1 - \lambda)f(x_2, y)] \\ &\leq \lambda[\max_{y \in \mathcal{Y}} f(x_1, y)] + (1 - \lambda)[\max_{y \in \mathcal{Y}} f(x_2, y)] \\ &= \lambda\psi(x_1) + (1 - \lambda)\psi(x_2), \end{aligned}$$

where the second inequality holds by convexity of $f(\cdot, y)$.

Moreover, we note that, since, for all $x \in \mathcal{X}$, $f(x, \cdot)$ is continuously differentiable on a compact convex set, every allowable path (with parameter $\varepsilon = 0$) can be extended to an allowable path whose endpoint \hat{y} has projected gradient $\nabla_y^{\mathcal{Y}} f(x^*, \hat{y}) = 0$.

Therefore, for every $(x, y) \in \mathcal{X} \times \mathcal{Y}$, there exists an allowable path with initial point y whose endpoint \hat{y} satisfies

$$\nabla_y^{\mathcal{Y}} f(x, \hat{y}) = 0. \tag{34}$$

Since $f(x, \cdot)$ is concave, (34) implies that

$$f(x, \hat{y}) = \max_{y \in \mathcal{Y}} f(x, y), \tag{35}$$

and hence that

$$\mathcal{L}_0(x, y) = f(x, \hat{y}). \quad (36)$$

Thus, (35) and (36) imply that

$$\mathcal{L}_0(x, y) = \psi(x) \quad \forall (x, y) \in \mathcal{X} \times \mathcal{Y} \quad (37)$$

since $\psi(x) = \max_{y \in \mathcal{Y}} f(x, y)$.

1. First we prove the “only if” direction:

Suppose that (x^*, y^*) is an approximate local equilibrium of f for our framework with respect to $\varepsilon = \delta = \omega = 0$ and the distribution Q . Let y^\dagger be a global maximizer of the function $f(x^*, \cdot)$ (the function achieves its global maximum since it is continuous and \mathcal{Y} is compact). Then the projected gradient at this point is

$$\nabla_y^{\mathcal{Y}} f(x^*, y^\dagger) = 0. \quad (38)$$

Since $f(x, \cdot)$ is concave for all x , and $\nabla_y^{\mathcal{Y}} f(x^*, y^*) = 0$, at every point y along the line $[y^\dagger, y^*]$ connecting the points y^\dagger and y^* , (38) implies that

$$\nabla_y^{\mathcal{Y}} f(x^*, y) = 0, \quad \forall y \in [y^\dagger, y^*]. \quad (39)$$

Therefore, (39) implies that

$$f(x^*, y^\dagger) = f(x^*, y^*),$$

and hence that

$$f(x^*, y^*) = \max_{y \in \mathcal{Y}} f(x^*, y), \quad (40)$$

since $\max_{y \in \mathcal{Y}} f(x^*, y) = f(x^*, y^\dagger)$.

Now, since (x^*, y^*) is an approximate local equilibrium with respect to $\varepsilon = \delta = \omega = 0$ and the distribution Q ,

$$\Pr_{\Delta \sim Q_{x^*, y^*}} [\mathcal{L}_0(x^* + \Delta, y^*) < \mathcal{L}_0(x^*, y^*)] = 0. \quad (41)$$

Thus, (37) and (41) together imply that

$$\Pr_{\Delta \sim Q_{x^*, y^*}} [\psi(x^* + \Delta) < \psi(x^*)] = 0. \quad (42)$$

Since ψ is convex, and since there is an open ball B for which Q_{x^*, y^*} has non-zero probability density at every point in $B \cap \mathcal{Y}$, (42) implies that x^* is a global minimizer for ψ :

$$\psi(x^*) = \min_{x \in \mathcal{X}} \psi(x). \quad (43)$$

Therefore, (40) and (43) imply that (x^*, y^*) is a global min-max point for $f : \mathcal{X} \times \mathcal{Y} \rightarrow \mathbb{R}$ whenever (x^*, y^*) is an approximate local equilibrium with respect to $\varepsilon = \delta = \omega = 0$ and the distribution Q .

2. Next, we prove the “if” direction:

Conversely, suppose that (x^*, y^*) is a global min-max point for $f : \mathcal{X} \times \mathcal{Y} \rightarrow \mathbb{R}$. Then $f(x^*, y^*) = \max_{y \in \mathcal{Y}} f(x^*, y)$. Since f is differentiable on $\mathcal{X} \times \mathcal{Y}$, this implies that

$$\nabla_y^{\mathcal{Y}} f(x^*, y^*) = 0. \quad (44)$$

Moreover, since $f(x^*, y^*)$ is a global min-max point, we also have that

$$f(x^*, y^*) = \min_{x \in \mathcal{X}} \left(\max_{y \in \mathcal{Y}} f(x, y) \right) = \min_{x \in \mathcal{X}} \psi(x),$$

and hence that

$$\psi(x^*) = \min_{x \in \mathcal{X}} \psi(x). \quad (45)$$

Since we have already shown that ψ is convex, (45) implies that

$$\Pr_{\Delta \sim Q_{x^*, y^*}} [\psi(x^* + \Delta) < \psi(x^*)] = 0. \quad (46)$$

Since we have also shown in (37) that $\psi(x) = \mathcal{L}_0(x, y)$ for all $(x, y) \in \mathcal{X} \times \mathcal{Y}$, (46) implies that

$$\Pr_{\Delta \sim Q_{x^*, y^*}} [\mathcal{L}_0(x^* + \Delta, y^*) < \mathcal{L}_0(x^*, y^*)] = 0. \quad (47)$$

Therefore, (44) and (47) imply that, (x^*, y^*) is an approximate local equilibrium for $f : \mathcal{X} \times \mathcal{Y} \rightarrow \mathbb{R}$ (with respect to $\varepsilon = \delta = \omega = 0$ and the distribution Q) whenever (x^*, y^*) is a global min-max point for f .

□

B Additional empirical details and results for Gaussian mixture and CIFAR-10 datasets

B.1 Simulation setup for Gaussian mixture and CIFAR-10 datasets

In this section we discuss the neural network architectures, choice of hyperparameters, and hardware used for both the real and synthetic data simulations.

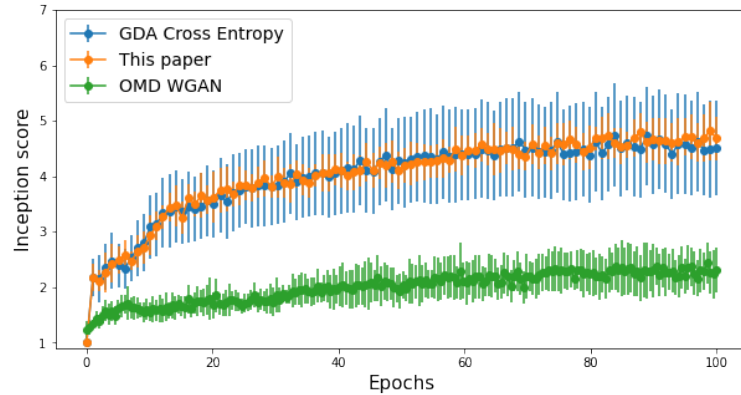


Figure 3: Inception score average (and standard deviation in errorbars) of all methods across iterations. Note that mean inception score of our algorithm is higher than the mean inception score of OMD, while the standard deviation of inception score of our algorithm is lower than the standard deviation of inception score of GDA.



Figure 4: GAN trained using our algorithm (with $k = 1$ discriminator steps and acceptance rate $e^{-1/\tau} = 1/2$). We repeated this simulation multiple times; here we display images generated from some of the resulting generators for our algorithm.



Figure 5: GAN trained using GDA (with $k = 1$ discriminator steps). We repeated this simulation multiple times; here we display images generated from some of the resulting generators for GDA.

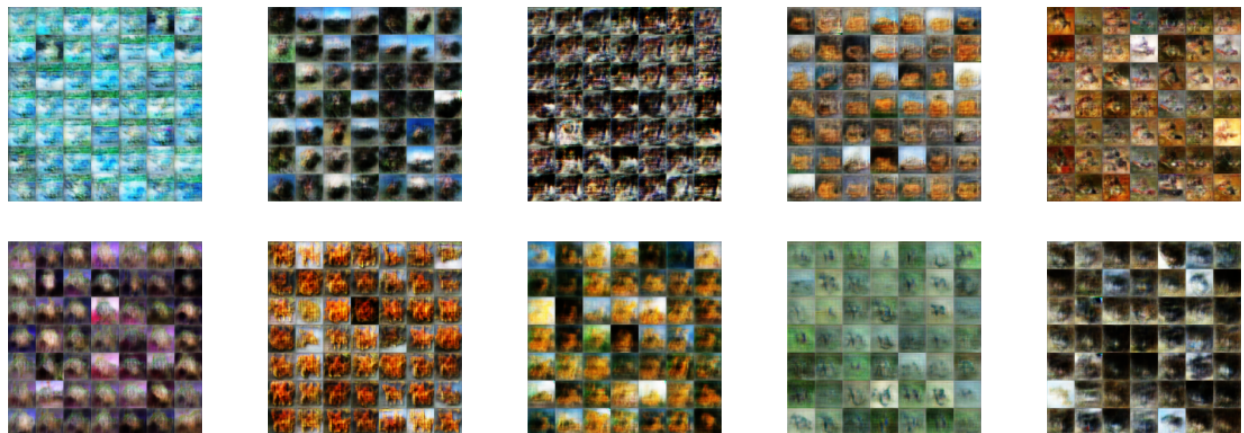


Figure 6: GAN trained using OMD. We repeated this simulation multiple times; here we display images generated from some of the resulting generators for OMD.

Hyperparameters for Gaussian mixture simulations. For the simulations on Gaussian mixture data, we have used the code provided by the authors of [27], which uses a batch size 512, Adam learning rates of 10^{-3} for the generator and 10^{-4} for the discriminator, and Adam parameter $\beta_1 = 0.5$ for both the generator and discriminator.⁵

We use the same neural networks that were used in the code from [27]: The generator uses a fully connected neural network with 2 hidden layers of size 128 and RELU activation, followed by a linear projection to two dimensions. The discriminator uses a fully connected neural network with 2 hidden layers of size 128 and RELU activation, followed by a linear projection to 1 dimension (which is fed as input to the cross entropy loss function). As in the paper [27], we initialize all the neural network weights to be orthogonal with scaling 0.8.

For OMD, we once again use Wasserstein loss and clip parameter 0.01.

Hyperparameters for CIFAR-10 simulations. For the CIFAR-10 simulations, we use a batch size of 128, with Adam learning rate of 0.0002 and hyperparameter $\beta_1 = 0.5$ for both the generator and discriminator gradients. Our code for the CIFAR-10 simulations is based on the code of Jason Brownlee [6], which originally used gradient descent ascent and ADAM gradients for training.

For the generator we use a neural network with input of size 100 and 4 hidden layers. The first hidden layer consists of a dense layer with 4,096 parameters, followed by a leaky RELU layer, whose activations are reshaped into 246 4×4 feature maps. The feature maps are then upscaled to an output shape of 32×32 via three hidden layers of size 128 each consisting of a convolutional *Conv2DTranspose* layer followed by a leaky RELU layer, until the output layer where three filter maps (channels) are created. Each leaky RELU layer has “alpha” parameter 0.2.

For the discriminator, we use a neural network with input of size $32 \times 32 \times 3$ followed by 5 hidden layers. The first four hidden layers each consist of a convolutional *Conv2DTranspose* layer followed by a leaky RELU layer with “alpha” parameter 0.2. The first layer has size 64, the next two layers each have size 128, and the fourth layer has size 256. The output layer consists of a projection to 1 dimension with dropout regularization of 0.4 and sigmoid activation function.

Setting hyperparameters. In our simulations, our goal was to be able to use the smallest number of discriminator or unrolled steps while still learning the distribution in a short amount of time, and we therefore decided to compare all algorithms using the same hyperparameter k . To choose this single value of k , we started by running each algorithm with $k = 1$ and increased the number of discriminator steps until one of the algorithms was able to learn the distribution consistently in the first 1500 iterations. This resulted in a choice of $k = 1$ for the MNIST datasets and a choice of $k = 6$ for the Gaussian mixture model data. For the CIFAR-10 dataset we simply used $k = 1$ for both algorithms (since for CIFAR-10 it is difficult to visually determine if all modes were learned).

Our temperature hyper-parameter was set by running our algorithm with temperatures in the set $\{1, 2, 3, 4, 5, 10\}$, and choosing the temperature which gave the best performance.

⁵Note that the authors also mention using slightly different ADAM parameters and neural network architecture in their paper than in their code; we have used the Adam parameters and neural network architecture provided in their code.

GDA with 1 discriminator step

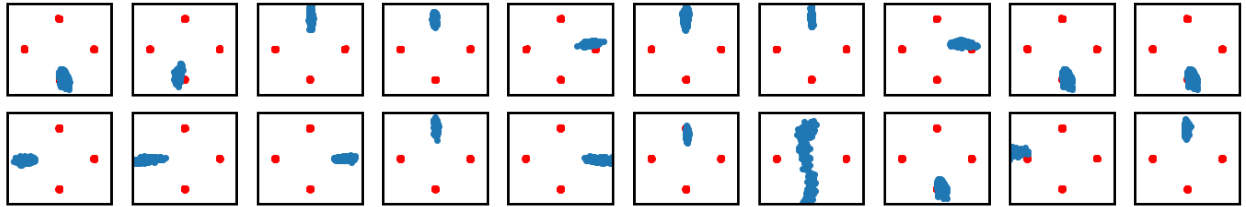


Figure 7: The generated points at the 1500'th iteration for all runs of GDA with $k = 1$ discriminator steps.

GDA with 6 discriminator steps

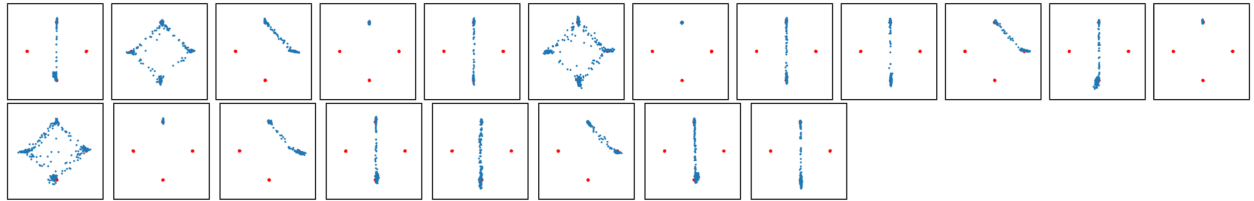


Figure 8: The generated points at the 1500'th iteration for all runs of the GDA algorithm, with $k = 6$ discriminator steps, for the simulation mentioned in Figure 1. At the 1500'th iteration, GDA had learned two modes 65% of the runs, one mode 20% of the runs, and four modes 15 % of the runs.

Hardware. Our simulations on the MNIST, 0-1 MNIST, and Gaussian mixture datasets were performed on four 3.0 GHz Intel Scalable CPU Processors, provided by AWS.

Our simulations on the CIFAR-10 dataset were performed on the above, and using one GPU with High frequency Intel Xeon E5-2686 v4 (Broadwell) processors, provided by AWS.

B.2 Additional simulation results for Gaussian mixture and CIFAR-10 datasets

In this section we show additional results for Gaussian mixture and CIFAR-10 datasets.

Our algorithm, GDA, and OMD trained on the CIFAR-10 dataset. In this section we show the results of additional runs of the simulations of our algorithm (Figure 4), GDA (Figure 5), and OMD (Figure 6), on the CIFAR-10 dataset, which were mentioned in Section 4. We also present the plot for mean of inception score across iterations for all three algorithms in Figure 3.

Comparison of algorithms on mixture of 4 Gaussians In this section we show the results of all the runs of the simulation mentioned in Figure 1, where all the algorithms were trained on a 4-Gaussian mixture dataset for 1500 iterations. For each run, we plot points from the generated distribution at iteration 1,500. Figure 7 gives the results for GDA with $k = 1$ discriminator step. Figure 8 gives the results for GDA with $k = 6$ discriminator steps. Figure 9 gives the results for the

Unrolled GANs with 6 unrolling steps

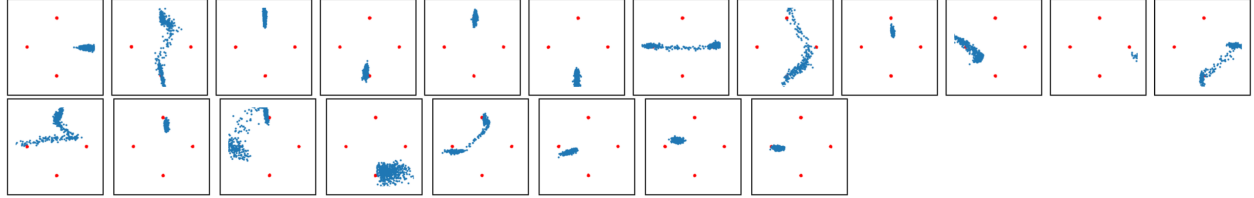


Figure 9: The generated points at the 1500'th iteration for all runs of the Unrolled GAN algorithm for the example in Figure 1, with $k = 6$ unrolling steps.

OMD

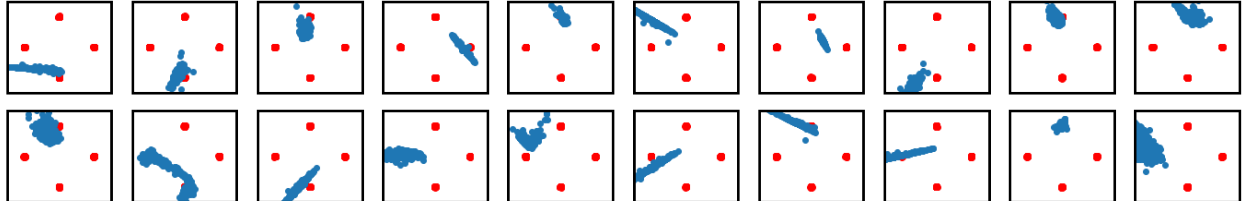


Figure 10: The generated points at the 1500'th iteration for all runs of OMD algorithm.

Unrolled GANs algorithm. Figure 10 gives the results for the OMD algorithm. Figure 11 gives the results for our algorithm.

C Empirical results for MNIST dataset

This dataset consists of 60k images of hand-written digits [22]. We use two versions of this dataset: the full dataset and the dataset restricted to 0-1 digits.

Our algorithm

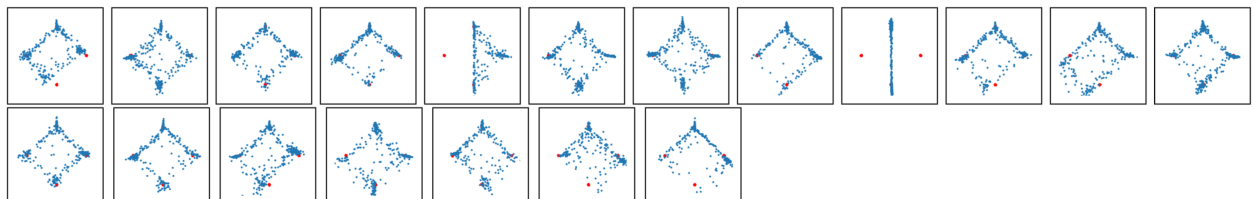


Figure 11: The generated points at the 1500'th iteration for all runs of our algorithm, for the simulation mentioned in Figure 1. Our algorithm used $k = 6$ discriminator steps and an acceptance rate hyperparameter of $\frac{1}{\tau} = \frac{1}{4}$. By the 1500'th iteration, our algorithm seems to have learned all four modes 70% of the runs, three modes 15% of the runs, and two modes 15% of the runs.

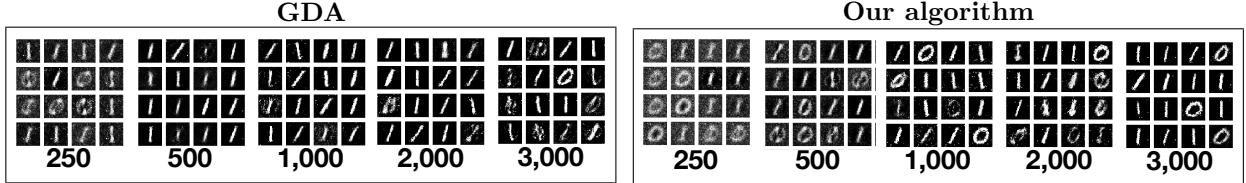


Figure 12: We trained a GAN using our algorithm on 0-1 MNIST for 30,000 iterations (with $k = 1$ discriminator steps and acceptance rate $e^{-1/\tau} = 1/5$). We repeated this experiment 22 times for our algorithm and 13 times for GDA. Shown here are the images generated from one of these runs at various iterations for our algorithm (right) and GDA (left).

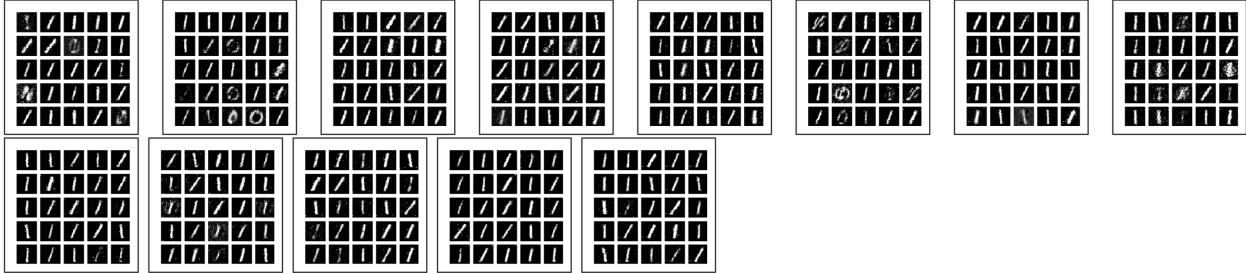


Figure 13: Images generated at the 1000’th iteration of the 13 runs of the GDA simulation mentioned in Figure 12. In 77% of the runs the generator seems to be generating only 1’s at the 1000’th iteration.

Hyperparameters for MNIST simulations. For the MNIST simulations, we use a batch size of 128, with Adam learning rate of 0.0002 and hyperparameter $\beta_1 = 0.5$ for both the generator and discriminator gradients. Our code for the MNIST simulations is based on the code of Renu Khandelwal [18] and Rowel Atienza [4], which originally used gradient descent ascent and ADAM gradients for training.

For the generator we use a neural network with input of size 256 and 3 hidden layers, with leaky RELUS each with “alpha” parameter 0.2 and dropout regularization of 0.2 at each layer. The first layer has size 256, the second layer has size 512, and the third layer has size 1024, followed by an output layer with hyperbolic tangent (“tanh”) activation.

For the discriminator we use a neural network with 3 hidden layers, and leaky RELUS each with “alpha” parameter 0.2, and dropout regularization of 0.3 (for the first two layers) and 0.2 (for the last layer). The first layer has size 1024, the second layer has size 512, the third layer has size 256, and the hidden layers are followed by a projection to 1 dimension with sigmoid activation (which is fed as input to the cross entropy loss function).

Results for 0-1 MNIST. We trained GANs using both GDA and our algorithm on the 0-1 MNIST dataset, and ran each algorithm for 3000 iterations (Figure 12). GDA seems to briefly generate shapes that look like a combination of 0’s and 1’s, then switches to generating only 1’s, and then re-learns how to generate 0’s. In contrast, our algorithm seems to learn how to generate both 0’s and 1’s early on and does not mode collapse to either digit. (See Figure 13 for images generated by all the runs of GDA, and 14 for images generated by the GAN for all the runs of our algorithm.)

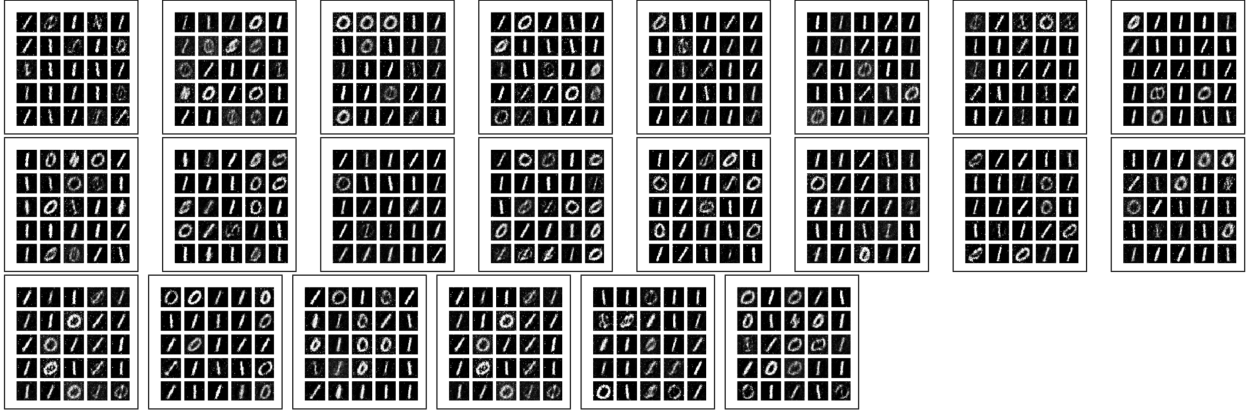


Figure 14: Images generated at the 1000'th iteration of each of the 22 runs of our algorithm for the simulation mentioned in Figure 12.

Full MNIST. Next we evaluate the utility of our algorithm on the full MNIST dataset. We trained a GAN on the full MNIST dataset using our algorithm for 39,000 iterations (with $k = 1$ discriminator steps and acceptance rate $e^{-1/\tau} = 1/5$). We ran this simulation five times; each time the GAN learned to generate all ten digits (see Fig. 15 for generated images).

D Randomized acceptance rule with decreasing temperature

In this section we give the simulations mentioned in the paragraph towards the beginning of Section 4, which discusses simplifications to our algorithm. We included these simulations to verify that our algorithm also works well when it is implemented using a randomized acceptance rule with a decreasing temperature schedule (Figure 16).

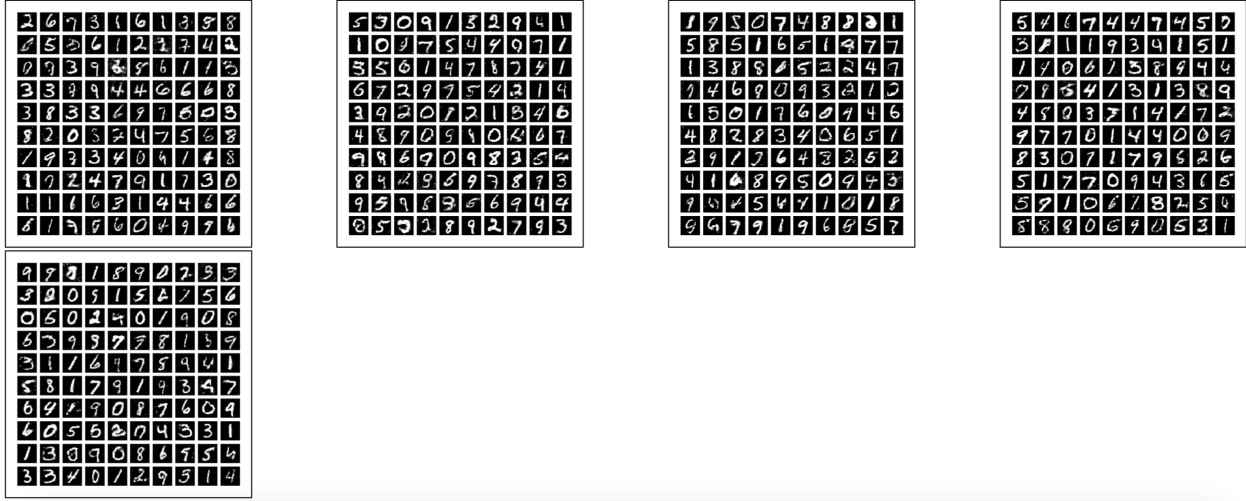


Figure 15: We ran our algorithm (with $k = 1$ discriminator steps and acceptance rate $e^{-\frac{1}{\tau}} = \frac{1}{5}$) on the full MNIST dataset for 39,000 iterations, and then plotted images generated from the resulting generator. We repeated this simulation five times; the generated images from each of the five runs are shown here.

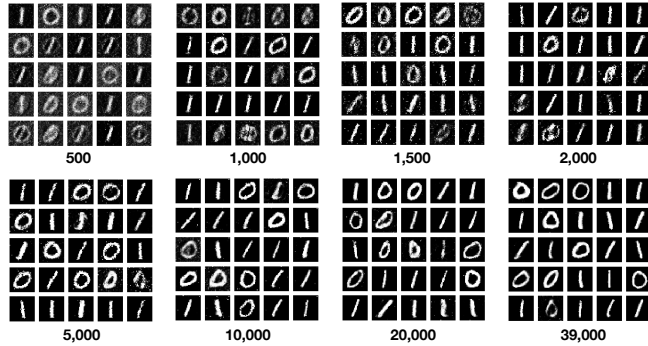


Figure 16: In this simulation we used a randomized accept/reject rule, with a decreasing temperature schedule. The algorithm was run for 39,000 iterations, with a temperature schedule of $e^{-\frac{1}{\tau_i}} = \frac{1}{4+e^{(i/20000)^2}}$. Proposed steps which decreased the computed value of the loss function were accepted with probability 1, and proposed steps which increased the computed value of the loss function were rejected with probability $\max(0, 1 - e^{-\frac{1}{\tau_i}})$ at each iteration i . We ran the simulation 5 times, and obtained similar results each time, with the generator learning both modes. In this figure, we plotted the generated images from one of the runs at various iterations, with the iteration number specified at the bottom of each figure (see also Figure 17 for results from the other four runs)

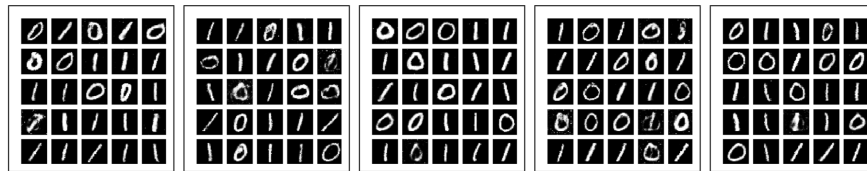


Figure 17: Images generated at the 39,000'th iteration of each of the 5 runs of our algorithm for the simulation mentioned in Figure 16 with a randomized acceptance rule with a temperature schedule of $e^{-\frac{1}{\tau_i}} = \frac{1}{4+e^{(i/20000)^2}}$.